
Discovering group dynamics in synchronous time series via hierarchical recurrent switching-state models

Michael Wojnowicz^{1,2}, Preetish Rath¹, Eric Miller¹, Jeffrey Miller², Clifford Hancock³, Meghan O’Donovan³, Seth Elkin-Frankston^{1,3}, Thaddeus Brunye^{1,3}, and Michael C. Hughes¹
¹Tufts University, ²Harvard University, ³US Army CCDC Soldier Center

Abstract

We seek to model a collection of time series arising from multiple entities interacting over the same time period. Recent work focused on modeling individual time series is inadequate for our intended applications, where collective system-level behavior influences the trajectories of individual entities. To address such problems, we present a new hierarchical switching-state model that can be trained in an unsupervised fashion to simultaneously explain both system-level and individual-level dynamics. We employ a latent system-level discrete state Markov chain that drives latent entity-level chains which in turn govern the dynamics of each observed time series. Feedback from the observations to the chains at both the entity and system levels improves flexibility via context-dependent state transitions. Our *hierarchical switching recurrent dynamical models* can be learned via closed-form variational coordinate ascent updates to all latent chains that scale linearly in the number of individual time series. This is asymptotically no more costly than fitting separate models for each entity. Experiments on synthetic and real datasets show that our model can produce better forecasts of future entity behavior than existing methods. Moreover, the availability of latent state chains at both the entity and system level enables interpretation of group dynamics.

1 Introduction

We consider the problem of jointly modeling a collection of time series. Each series in the collection describes the evolution of one *entity* within a shared environment or *system* containing multiple interacting entities observed over the same time period. Our work is motivated by the need to capture

an essential property of such data in many applications: the temporal behaviors of the individual entities are *coordinated* in a systematic but fundamentally latent (i.e., unobserved) manner. For example, consider the dynamics of a team sport like basketball [Terner and Franks, 2021]. One player might set a screen to allow a teammate to drive to the basket. As another example, consider a squad of soldiers engaged in a training exercise. They must work together to protect their blindsides from attack while accomplishing their mission. In both examples, the dynamics of the individuals are far from independent. Instead, the observed trajectories exhibit “top-down” patterns of coordination learned from extensive training together as well as “bottom-up” adaptations of the individuals and the group to evolving situational demands. We seek to build a model that can infer how group dynamics evolve over time given only entity-level sensory measurements, while taking into account top-down and bottom-up influences. We return to the soldiers later in Sec. 5.3 and to basketball in Sec. 5.2. Similar group dynamics arise in many other domains, such as the behavior of businesses in a shared economic system [van Dijk et al., 2002] or animals in a shared habitat [Sun et al., 2021].

While modeling individual time series has seen many recent advances [Farnoosh et al., 2021, Gu et al., 2022, Linderman et al., 2017], there remains a need for improved models for coordinated collections of time series. Among works that try to model collections of time series, the simplest approaches repurpose models for individual time series, either fitting separate models to individual entities or pooling all entities together as iid observations from one common model. As a step beyond this, some efforts pursue *personalized* models that allow custom parameters that govern each entity’s dynamics while sharing information between entities via common priors on these parameters [Alaa and van der Schaar, 2019, Linderman et al., 2019, Severson et al., 2020], often using mixed effects [Altman, 2007, Liu et al., 2011]. But personalized models allow each sequence to unfold asynchronously, without interaction over time. In contrast, our goal is to develop models specifically capable of capturing the synchronously coordinated behavior of a group of interacting entities in the same time period. Others

have pursued this goal with complex neural architectures that can jointly model “multi-agent” trajectories [Alcorn and Nguyen, 2021, Xu et al., 2022, Zhan et al., 2019]. Instead, we focus on parametric methods that are easier to interpret for stakeholders and more likely to fit well in applications with only a few minutes of available data (such as Sec. 5.3).

One potential barrier to modeling synchronous coordination across entities is computational complexity. For instance, a model with discrete hidden states which allows interactions among entities has a factorial structure with inference that scales *exponentially* in the number of entities (see Sec. 3). In this paper we present a tractable framework for modeling collections of synchronous time series that overcomes this barrier. All estimation can be done with cost linear in the number of entities, making our model’s asymptotic runtime complexity no more costly than fitting separate models to each entity.

Our **first key modeling contribution** is an explicit representation of the *hierarchical* structure of group dynamics, using switching-state models [Rabiner, 1989] as a building block. As shown in Fig. 1, our model posits two levels of latent discrete state chains: a system-level chain (shared by all entities) and an entity-level chain unique to each entity. We assume that the system-level state is the sole mediator of cross-entity coordination; each entity-level chain is conditionally independent of other entities given the system-level state chain. Our model achieves “top down” patterns of coordination via the system-level chain’s influence on each entity-level chain’s state transition dynamics. In turn, our model generates observed time series via an emission model conditioned on the entity-level chain.

The **second key modeling contribution** is to allow the transition probabilities among states *at all levels* to depend on feedback from observations at the previous timestep. Such feedback provides a natural means of modeling the inherent context dependence of the state transitions, allowing “bottom up” reactions to situational demands. In the basketball context, this feedback captures how a basketball player driving to the basket will switch to another behavior once they reach their goal and how this switch may influence the trajectories of the others on the team. Previously, Linderman et al. [2017] incorporated this *recurrent* feedback into a model with a flat single-level of switching states. We show how recurrent feedback can inform a two-level hierarchy of system-level and entity-level states, so that entity-level observations can drive system-level transitions.

Our overall contribution is thus a proposed framework – *hierarchical switching recurrent dynamical models* – by which our two key modeling ideas provide a natural solution to the problem of unsupervised modeling of time series arising from a group of interacting entities. Unlike other models, our framework allows each entity’s next-step dynamics to be driven by both a system-level discrete state (“top-down” in-

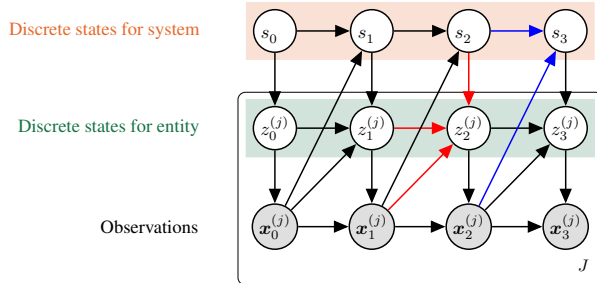


Figure 1: *Graphical model representation of our proposed hierarchical switching recurrent dynamical model (HSRDM) for a system of J interacting entities.* The colored edges highlight the key insights behind our flexible transition models of system-level hidden states s and entity-level hidden states z . Transitions to the next system state depend (via blue arrows) on the current system state and recurrent feedback from observations of all entities (up-diagonal blue). Transitions to the next entity state depend (via red arrows) on the next system-level state (down), the current entity state (horizontal), and recurrent feedback from entity observations (up-diagonal red).

fluence) and recurrent feedback from previous observations (“bottom-up” influence). Optional exogenous features (e.g. the ball position in basketball) can also be easily incorporated. We further provide a variational inference algorithm for simultaneously estimating model parameters and approximate posteriors over system-level and entity-level chains. Each chain’s posterior maintains the model’s temporal dependency structure while remaining affordable to fit via efficient dynamic programming that incorporates recurrent feedback. We conduct experiments on a synthetic dataset as well as two real-world tasks: modeling player positions in a professional basketball game and modeling soldier headings in a simulated training exercise. Compared to recent single-level switching-state baselines, our hierarchical approach can produce better forecasts and reveal interpretable group dynamics, even when baselines are allowed flexible transitions and emissions via neural networks.

2 Model Family

Here we present a family of *hierarchical switching recurrent dynamical models* (HSRDMs) to describe a collection of time series gathered from J entities that interact over a common time period (discretized into timesteps $t \in \{0, 1, 2, \dots, T\}$) and in a common environment or *system*. For each entity, indexed by $j \in \{1, \dots, J\}$, we observe a time series of feature vectors $\{\mathbf{x}_t^{(j)} \in \mathbb{R}^D, t = 0, 1, 2, \dots, T\}$.

Our HSRDM represents the j -th entity via two random variables: the observed features $\mathbf{x}_{0:T}^{(j)}$ above and a hidden entity-level discrete state sequence $z_{0:T}^{(j)} = \{z_t^{(j)} \in \{1, \dots, K_j\}, t = 0, \dots, T\}$. We further assume a system-level latent time series of discrete states

$s_{0:T} = \{s_t \in \{1, \dots, L\}, t = 0, \dots, T\}$. The complete joint of all random variables, as diagrammed in Figure 1, factorizes as

$$\begin{aligned}
 p(\mathbf{x}_{0:T}^{(1:J)}, z_{0:T}^{(1:J)}, s_{0:T} | \theta) &= \underbrace{p(s_0 | \theta)}_{\text{initial system state}} \prod_{t=1}^T \underbrace{p(s_t | s_{t-1}, \mathbf{x}_{t-1}^{(1:J)}, \theta)}_{\text{system state transitions}} \\
 &\cdot \prod_{j=1}^J \left[\underbrace{p(z_0^{(j)} | s_0, \theta)}_{\text{initial entity state}} \prod_{t=1}^T \underbrace{p(z_t^{(j)} | z_{t-1}^{(j)}, \mathbf{x}_{t-1}^{(j)}, s_t, \theta)}_{\text{entity state transitions}} \right. \\
 &\cdot \left. \underbrace{p(\mathbf{x}_0^{(j)} | z_0^{(j)}, \theta)}_{\text{initial obs.}} \prod_{t=1}^T \underbrace{p(\mathbf{x}_t^{(j)} | \mathbf{x}_{t-1}^{(j)}, z_t^{(j)}, \theta)}_{\text{observation dynamics}} \right] \quad (2.1)
 \end{aligned}$$

where θ represent all model parameters, and superscript $(1:J)$ denotes the union over all entities.

The design principle of HSRDMs is to coordinate the switching-state dynamics of multiple entities so they receive top-down influence from system-level state as well as bottom-up influence via recurrent feedback from entity observations. Under the generative model, the next entity-level state depends on the interaction of three sources of information: the next state of the system, the current state of the entity, and the current entity observation. Likewise, the next system state depends on the current system state and observations from *all* entities.

Transition models. To instantiate our two-level discrete state transition distributions, we use categorical generalized linear models to incorporate each source of information via additive utilities

$$s_t | s_{t-1}, \mathbf{x}_{t-1}^{(1:J)} \sim \text{Cat-GLM}_L \left(\underbrace{\tilde{\Pi}^T e_{s_{t-1}}}_{\text{transitions}} + \underbrace{\Lambda g_\psi(\mathbf{x}_{t-1}^{(1:J)}, \mathbf{v}_{t-1})}_{\text{recurrence}} \right) \quad (2.2)$$

$$z_t^{(j)} | z_{t-1}^{(j)}, \mathbf{x}_{t-1}^{(j)}, s_t \sim \text{Cat-GLM}_K \left(\underbrace{(\tilde{\mathbf{P}}_j^{(s_t)})^T e_{z_{t-1}^{(j)}}}_{\text{transitions}} + \underbrace{\Psi_j^{(s_t)} f_\phi(\mathbf{x}_{t-1}^{(j)}, \mathbf{u}_{t-1}^{(j)})}_{\text{recurrence}} \right) \quad (2.3)$$

Across levels, common sources of information drive these utilities. First, the *state-to-state transition* term selects an appropriate log transition probability vector from matrices $\tilde{\Pi}, \tilde{\mathbf{P}}$ via a one-hot vector e_k indicating the previous state k . Second, *recurrent feedback* governs the next term, via featurization functions for the system $g_\psi : \mathbb{R}^{DJ} \rightarrow \mathbb{R}^{\tilde{R}}$ and for entities $f_\phi : \mathbb{R}^D \rightarrow \mathbb{R}^{\tilde{D}}$ with parameters ψ, ϕ (known or learned) and weights Λ, Ψ_j . If optional *exogenous covariates* are available at either the system-level in \mathbf{v}_{t-1} or entity-level in $\mathbf{u}_{t-1}^{(j)}$, they can also drive the transition probabilities. Note that inference (Sec. 3) applies not merely to Eq. (2), but to arbitrary instantiations.

Emission model. We generate the next observation for entity j via a state-conditioned autoregression:

$$\mathbf{x}_t^{(j)} | \mathbf{x}_{t-1}^{(j)}, z_t^{(j)} \sim H_\zeta \quad \text{where } \zeta = \zeta(\mathbf{x}_{t-1}^{(j)}, z_t^{(j)}). \quad (2.4)$$

Users can select distribution H to match the domain of observed features $\mathbf{x}_t^{(j)}$: our later experiments use Gaussians for real-valued vectors and Von-Mises distributions for angles. The parameter $\zeta = \zeta(\mathbf{x}_{t-1}^{(j)}, z_t^{(j)})$ depends on the previous observation $\mathbf{x}_{t-1}^{(j)}$ and current entity-level state $z_t^{(j)}$.

Priors. The Appendix describes prior distributions $p(\theta)$ on parameters assumed for the purpose of regularization. We use a ‘‘sticky’’ Dirichlet prior [Fox et al., 2011] to obtain smoother segmentations at the system level.

Specification. To apply HSRDM to a concrete problem, a user must select the number of system states L and entity states K as well as functional forms of g, f . We assume that g can be evaluated in $\mathcal{O}(J)$.

Special cases. If we remove the top-level system states $s_{0:T}$ (or equivalently set $L = 1$), our HSRDM reduces to Linderman et al. [2017]’s recurrent autoregressive HMM (rAR-HMM). If we removed recurrent and covariate terms from the transition model, we’d recover a multi-level HMM.

3 Inference

Given observed time series $\mathbf{x}_{0:T}^{(1:J)}$, we now explain how to simultaneously estimate parameters θ and infer approximate posteriors over hidden states $s_{0:T}$ for the system and $z_{0:T}^{(1:J)}$ for all J entities. Because all system-level and entity-level states are unobserved, the marginal likelihood $p(\mathbf{x}_{0:T} | \theta)$ is a natural objective for parameter estimation. However, exact computation of this quantity, by marginalizing over all hidden states, is intractable. Given L system-level states and K entity-level states, computing $p(\mathbf{x}_{0:T} | \theta)$ naively via the sum rule requires a sum over $(LK^J)^T$ values. While the forward algorithm [Rabiner, 1989] resolves the exponential dependence in time, the exponential dependence in the number of entities persists: TLK^{2J} operations are required to do forward-backward on HSRDMs. This exponential dependence makes inference prohibitively costly even in moderate settings; for instance, when $(T^*, J^*, L^*, K^*) = (100, 10, 2, 4)$, a direct application of the forward algorithm still requires around 220 trillion operations.

Instead, we will pursue a structured approximation q to the true (intractable) posterior over hidden states. Following previous work [Alameda-Pineda et al., 2021, Linderman et al., 2017], we define

$$q(s_{0:T}, z_{0:T}^{(1:J)}) = q(s_{0:T}) q(z_{0:T}^{(1:J)}), \quad (3.1)$$

intending $q(s_{0:T}, z_{0:T}^{(1:J)}) \approx p(s_{0:T}, z_{0:T}^{(1:J)} | \mathbf{x}_{0:T}^{(1:J)}, \theta)$. Each factor retains temporal dependency structure, avoiding the problems of complete mean-field inference [Barber et al.,

2011]. Using this q , we can form a variational lower bound on the marginal log likelihood $\text{VLBO} \leq \log p(\mathbf{x}_{0:T}^{(1:J)})$, defined as $\text{VLBO}[\theta, q] = \mathbb{E}_q[\log p(\mathbf{x}_{0:T}^{(1:J)}, z_{0:T}^{(1:J)}, s_{0:T}, \theta)] + \mathbb{H}[q(z_{0:T}^{(1:J)}, s_{0:T})]$.

As shown in the Appendix, computation of this bound scales as $O(TJL^2K^2)$, crucially *linear* rather than exponential in the number of entities J . This reduces the approximate number of operations required for inference on (T^*, J^*, L^*, K^*) from 220 trillion to 64 thousand.

To estimate θ and q given data $\mathbf{x}_{0:T}$, we pursue coordinate ascent variational inference (CAVI; [Blei et al., 2017]) on the VLBO (known as variational expectation maximization [Beal, 2003] when θ is approximated with a point mass). Given a suitable initialization, we alternate between the updates:

$$\begin{aligned} q(z_{0:T}^{(1:J)}) &\propto \exp \left\{ \mathbb{E}_{q(s_{0:T})} [\log p(\mathbf{x}_{0:T}^{(1:J)}, z_{0:T}^{(1:J)}, s_{0:T} | \theta)] \right\} \\ q(s_{0:T}) &\propto \exp \left\{ \mathbb{E}_{q(z_{0:T}^{(1:J)})} [\log p(\mathbf{x}_{0:T}^{(1:J)}, z_{0:T}^{(1:J)}, s_{0:T} | \theta)] \right\} \\ \theta &= \underset{\theta}{\operatorname{argmax}} \left\{ \mathbb{E}_{q(z_{0:T}^{(1:J)})q(s_{0:T})} \left[\log p(\mathbf{x}_{0:T}^{(1:J)}, z_{0:T}^{(1:J)}, s_{0:T} | \theta) \right] + \log p(\theta) \right\} \end{aligned} \quad (3.2)$$

which give the variational E-Z step (VEZ step), variational E-S step (VES step), and M-step, respectively. All steps will improve the VLBO objective provided each improves its own per-step objective.

VES step for system-level state posteriors. We can show the VES step reduces to updating the posterior of one Hidden Markov Model with J independent autoregressive categorical emissions. Optimal variational parameters for this posterior can be computed via a dynamic-programming algorithm that extends classic forward-backward for an AR-HMM to handle recurrence. The runtime required is $O(TJ(K^2 + KD + KL + KM) + TL^2)$.

VEZ step for entity-level state posteriors. We can show that the VEZ update can reduce to a separate Hidden Markov Model for each entity j with autoregressive categorical emissions which recurrently feedback into the transitions. Given a fixed system-level factor $q(s_{0:T})$, we can update the state posterior for entity j independently of all other entities. This means inference is *linear* in the number of entities J , despite the fact that the HSRDM couples entities via the system-level sequence. The linearity arises even though our assumed mean-field variational family of Eq. (3.1) did not make an outright assumption that $q(z_{0:T}^{(1:J)}) = \prod_{j=1}^J q(z_{0:T}^{(j)})$. Optimal variational parameters for this posterior can again be computed by dynamic programming. The runtime required to update each entity’s factor is $O(T[K^2 + KD^2 + KL + KM])$.

M step for transition/emission parameters. Updates to some parameters, particularly for emission model parameters when H has exponential family structure (such as the Gaussian or Von-Mises AR likelihoods we use throughout experiments), can be done in closed-form. Otherwise, in general, we optimize θ by gradient ascent on the VLBO objective. This has the same cost as the computation of the VLBO, with runtime $O(TJL^2K^2)$.

Full details about each step, as well as recommendations for initialization, are in the Appendix. We also share code (built upon JAX for automatic differentiation [Bradbury et al., 2018]).

4 Related Work

Below we review several threads of the scientific literature in order to situate our work.

Continuous representations of individual sequences. Other efforts focus on latent continuous representations of individual time series. These can produce competitive predictions, but do not share our goal of providing a segmentation at the system and entity level into distinct and interpretable regimes. Probabilistic models with continuous latent state representations are often based on classic linear dynamical system (LDS) models [Shumway and Stoffer, 1982]. Deep generative models like the Deep Markov Model [Krishnan et al., 2017] and DeepState [Rangapuram et al., 2018] extend the LDS approach with more flexible transitions or emissions via neural networks.

Discrete state representations of individual sequences. Our focus is on discrete state representations which provide interpretable segmentations of available data, a line of work that started with classic approaches to entity-level-only sequence models like hidden Markov models or switching-state linear dynamical systems (SLDS) [Alameda-Pineda et al., 2021, Ghahramani and Hinton, 2000]. Recent efforts such as DSARF [Farnoosh et al., 2021], SNLDS [Dong et al., 2020] and DS3M [Xu and Chen, 2021] have extended such base models to non-linear transitions and emissions via neural networks. All these efforts still represent each time series via one entity-level discrete state sequence.

Discrete states via recurrence on continuous observations. Linderman et al. [2017] add a notion of *recurrence* to classic SLDS models, increasing the flexibility in each timestep’s transition distribution by allowing dependence on the previous continuous features, not just the previous discrete states. Later work has extended recurrence ideas in several directions that improve entity-level sequence modeling, such as multi-scale transition dependencies via the tree-structured construction of the TrSLDS [Nassar et al., 2019] or recurrent transition models that can explicitly model state durations via RED-SDS [Ansari et al., 2021]. To model multiple recordings of worm neural activity, Linderman et al. [2019] pursue recurrent state space models that are

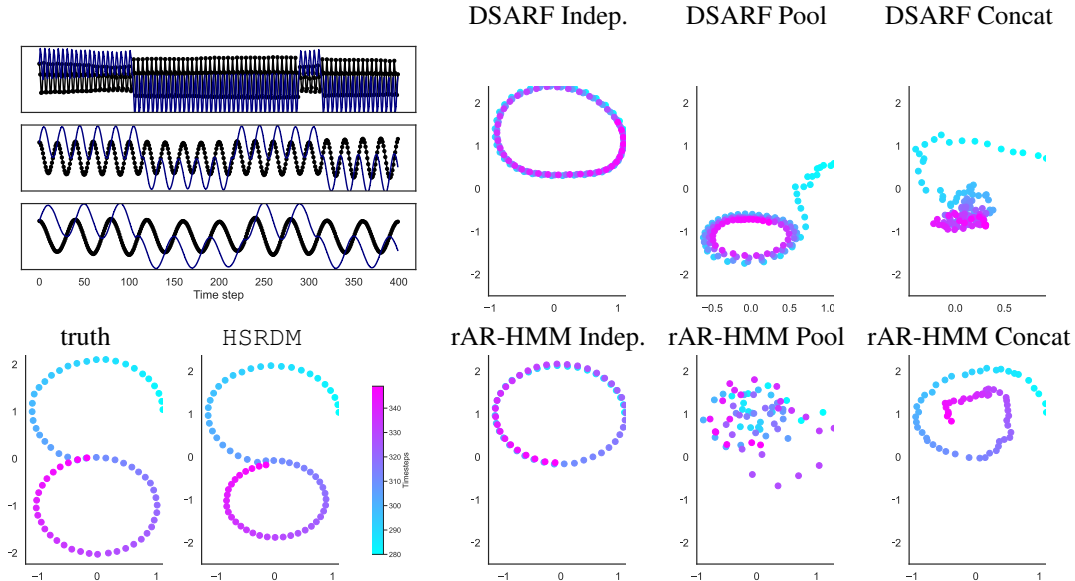


Figure 2: Comparing model predictions of heldout time segment of one entity in *Figure Eight* task. **Top left:** Data generating process. Each panel gives the (x,y) coordinates from one entity. Models were trained on all data from entities 1-2 and times 0-280 for entity 3, then asked to forecast times 281 onward for entity 3. **Bottom left:** Our HSRDM predictions closely matches truth in all 3 samples. **Bottom right:** Best sample for rAR-HMM baseline, under each possible strategy (Indep., Pool, and Concat., defined in Sec. 5.1) for adapting an entity-only model to our hierarchical setting. **Top right:** Best of 3 samples from DSARF baseline under each strategy. See App. for further visuals.

described as *hierarchical* because they encourage similarity between each worm entity’s custom dynamics model via common parameter priors in hierarchical Bayesian fashion. Their model assumes only entity-level discrete states.

Multi-level discrete representations. Stanculescu et al. [2014] developed a hierarchical switching linear dynamical system (HSLDS) for modeling the vital sign trajectories of individual infants in an intensive care unit. The root level of their directed graphical model assumes a discrete state sequence (analogous to our s) indicating whether disease was present or absent in the individual over time, while lower level discrete states (analogous to our z) indicate the occurrence of specific “factors” representing clinical events such as bradycardia or desaturation. While their graphical model looks similar to ours in its multi-level discrete structure, we emphasize three key differences. First, they model individual time series not multiple interacting entities. Second, they assume fully-supervised data for training, where each timestep t is *labeled* with top-level and factor-level states. In contrast, our structured VI routines to estimate parameters in the unsupervised setting are new. Finally, their HSLDS does not incorporate recurrent feedback from continuous observations.

More broadly, Hierarchical Hidden Markov Models (HHMMs) [Fine et al., 1998] and their extensions [Bui et al., 2004, Heller et al., 2009] describe a single entity’s observed sequence with multiple levels of hidden states. The chief motivation of the HHMM is to model different temporal

length scales of dependency within an individual sequence. While HHMMs have been applied widely to applications like text analysis [Skounakis et al., 2003] or human behavior understanding [Nguyen et al., 2005], to our knowledge HHMMs have not been used to coordinate multiple overlapping in time.

Models of teams in sports analytics. Turner and Franks [2021] survey approaches to player-level and team-level models in basketball. Miller and Bornn [2017] apply topic models to tracking data to discover how low-level actions (e.g. run-to-basket) might co-occur among teammates during the same play. Metulini et al. [2018] model the convex hull formed by the court positions of the 5-player team throughout a possession via one system-level hidden Markov model. In contrast, our work provides a coordinated two-level segmentation representing the system as well as individuals.

Personalized models. Several switching state models assume each sequence in a collection have unique or personalized parameters, such custom transition probabilities or emission distributions [Alaa and van der Schaar, 2019, Fox et al., 2014, Severson et al., 2020]. In this style of work, entity time series may be collected asynchronously, and entities are related by shared priors on their parameters. In contrast, we focus on entities that are synchronous in the same environment, and relate entities directly via a system-level discrete chain that modifies entity-level state transitions.

Models of coordinated entities. Several recent methods do jointly model multiple interacting entities or “agents”, often using sophisticated neural architectures. Zhan et al. [2019] develop a variational RNN where trajectories are coordinated in short time intervals via entity-specific latent variables called “macro-intents”. Yuan et al. [2021] develop the AgentFormer, a transformer-inspired stochastic multi-agent trajectory prediction model. Alcorn and Nguyen [2021] develop baller2vec++, a transformer specifically designed to capture correlations among basketball player trajectories. Xu et al. [2022] introduce GroupNet to capture pairwise and group-wise interactions. Unlike these approaches, ours builds upon switching-state models with *closed-form* posterior inference, produces *discrete* segmentations, and may be more sample efficient for applications like Sec. 5.3 with only a few minutes of data.

Models that learn interaction graphs. Some works [Kipf et al., 2018, Sanchez-Gonzalez et al., 2020] pursue the goal of learning an interaction graph given many entity-level time series, where nodes correspond to entities and edge existence implies a direct, pairwise interaction between entities. For some applications, discovering pairwise interactions is an interesting goal. In our chosen applications (e.g. the simulated battle exercises or basketball player movements), we hypothesize that the graph will always be fully-connected. Moreover, interaction graph approaches burdensomely require runtimes that are quadratic in the number of entities J on our fully-connected applications. In contrast, our approach models the system-level group dynamics explicitly while keeping the cost of processing scalably linear in J .

5 Experiments

We now compare our proposed model to several alternatives in terms of quantitative performance (via short-term multi-step-ahead forecasting error), as well as qualitative performance at inferring useful discrete representations of system-level and entity-level dynamics. As a representative of sophisticated neural architectures for coordinated entities, we selected AgentFormer [Yuan et al., 2021], due to its available code that supports multi-step forecasting. Unfortunately, the baller2vec codebase [Alcorn and Nguyen, 2021] only supports one-step-ahead forecasting as of this writing.

We further selected two competitive baselines that only capture entity-level dynamics (not system-level) but still infer entity-level discrete segmentations. First, we compare to a recurrent autoregressive hidden Markov model (rAR-HMM; [Linderman et al., 2017]). This is essentially an ablation of our method that removes our hierarchy. Second, we compare to the deep switching autoregressive factorization model (DSARF; [Farnoosh et al., 2021]), which we chose as a representative of models that infer discrete latent segmentations while also reporting state-of-the-art forecasting performance against recent alternatives and using deep neural networks to flexibly define transition and emission

structures. For each rAR-HMM and DSARF, we try three different strategies for modeling a system of entities. First, *complete independence* (“*Indep.*”), where a separate model is fit to each entity. Next, *complete pooling* (“*Pool*”), where one single model is fit on all data, treating each entity’s time series as an *i.i.d* observation. Finally, *concatentation* (“*Concat.*”), which fits one model to one multivariate time series of expanded dimension $D' = J \cdot D$ constructed by stacking up all entity-specific features $\mathbf{x}_t^{(1)}, \mathbf{x}_t^{(2)}, \dots, \mathbf{x}_t^{(J)}$ at each time t .

5.1 FigureEight: Synthetic task of coordinated dynamics over time

To illustrate the potential of our HSRDM as a model for coordinated group dynamics, we study a synthetic dataset we call *FigureEight*. In the true generative process (detailed in Appendix), each entity switches between clockwise motion around a top loop and counter-clockwise motion around a bottom loop, so the observed entity-level 2D spatial trajectory over time approximates the shape of an “8”. The trajectories of the entities for each loop is governed by a Gaussian vector autoregression process. Transition between these loop states depend on entity-level recurrent feedback (switches between loops are only probable near the origin, where the loops intersect) and crucially on a binary system-level state (which sets which loop is favored for all entities at the moment). Though coordinated, entity trajectories are not perfectly synchronized, varying due to individual rotation speeds, initial positions, and random effects (visuals in Appendix).

Given a dataset of three entities observed together for 280 timesteps, we pursue *partial forecasting* (Sec. C.2) of one target entity’s remaining trajectory for times 281-350, given fully observed trajectories from the other two entities. The true target trajectory for this heldout window is illustrated in Fig. 2: we see a smooth transition from the top loop to the bottom loop. Each tested method is evaluated by how well its generated sample trajectories for the heldout period adequately match the true heldout behavior from the generative process.

We apply our HSRDM with entity-level recurrence f set to a radial basis function. For simplicity, we do not use system-level recurrence g . While we do not expect recurrence to improve training fit, we do expect it to improve forecasting, as it is necessary to capture a key aspect of the true process: that switches between loops are only probable near the origin. Reproducible details for our method and all alternative methods (architectures, training, and hyperparameters) are in the Appendix.

Fig. 2 visualizes the best sample forecast of 3 for each baseline, as well as the worst forecast of 3 from our HSRDM. While our proposed model provides a natural fit, the baseline models struggle to reproduce the coordinated group dynamics.

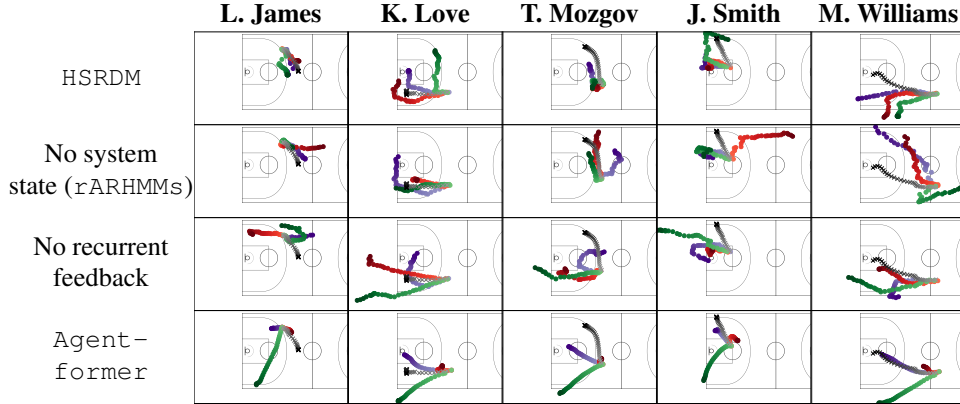


Figure 3: *Sample forecasts of NBA player location trajectories.* Shown in grey are true player trajectories from the forecasting window of the test event on which our model had median forecasting error. In color are three sampled forecasts from each model; purple/red/green has 1st/5th/10th best forecasting error (from 20 samples). Time runs from light to dark.

5.2 Forecasting 2D position trajectories of all 10 players in pro basketball games

We next model the 5 players of the NBA’s Cleveland Cavaliers (CLE), together with their 5 opponents, across multiple games in an open-access dataset [Linou, 2016] of player positions over time recorded from CLE’s 2015-2016 championship season. We focused exclusively on the 29 games involving one of CLE’s four most common starting lineups. We randomly assigned these games to training (20 games), validation (4 games), and test (5 games) sets.

We split each game into non-overlapping basketball *events*, typically lasting 20 seconds to 3 minutes. Events concatenate consecutive *plays* (e.g. shot block → rebound offense → shot made) from the raw dataset until there is an abrupt break in player motion or a sampling interval longer than the nominal sampling rate. Each event gives an (x, y) court position for all 10 players, and is modeled as an i.i.d. sequence from our proposed HSRDM or competitor models. We standardized the court so that CLE’s offense always faces the same direction (left), and downsampled the data to 5 Hz.

Our system-level recurrence g reports *all* player locations $\mathbf{x}_t^{(1:J)}$ to the system-level transition function, allowing the probability of latent game states to depend on player locations. Following Linderman et al. [2017], our entity-level recurrence function f reports an individual player’s location $\mathbf{x}_t^{(j)}$ (and out-of-bounds indicators) to that player’s entity-level transition function, allowing each player’s probability of remaining in autoregressive regimes to vary in likelihood over the court. Finally, our emissions distribution is a Gaussian vector autoregression with entity-state-dependent parameters (see Sec. F).

We compare the forecasting performance of the HSRDM to multiple competitors: AgentFormer [Yuan et al., 2021]; an ablation of the system-level switches, which gives in-

Table 1: *Forecasting NBA player trajectories.*

	Mean forecasting error (in feet) after n training games		
	$n = 1$	$n = 5$	$n = 20$
HSRDM (ours)	16.3 (–)	14.4 (–)	14.4 (–)
No system state (rARHMM)	15.9 (0.2)	15.5 (0.2)	15.6 (0.2)
No recurrent feedback	16.6 (0.3)	16.0 (0.2)	16.3 (0.2)
Fixed velocity	16.8 (0.5)	16.8 (0.4)	16.8 (0.4)
AgentFormer	33.5 (0.4)	21.2 (0.6)	25.8 (0.3)

dependent rARHMMs [Linderman et al., 2017] for each player; and an ablation of the recurrent feedback. As in Yeh et al. [2019], we also try a crude but often competitive *fixed velocity* baseline. Training HSRDM on a 2023 Macbook with Apple M2 Pro chip on $n = 1, 5, 20$ training games took 2, 15, and 45 minutes, respectively. Training AgentFormer on an Intel Xeon Gold 6226R CPU took 1.5, 6, and 13 hours, respectively.

To evaluate methods, we randomly select a 6 second forecasting window within each of the 75 test set events. Preceding observations in the event are taken as context, and postceding observations are discarded. We sample 20 forecasts from each method. Tab. 1 reports the mean distance in feet from forecasts to ground truth, with the mean taken over all events, samples, players, timesteps, and dimensions. We perform paired t-tests on the per-event differences in mean distances between our model vs competitors, using Benjamini and Hochberg [1995]’s correction for multiple comparisons over positively correlated tests. The standard errors for the mean differences are given in parentheses. Methods whose forecasting performance are not statistically significantly different from HSRDM at the .05 level are given in bold. We find that HSRDM provides better forecasts than AgentFormer and fixed velocity, and that HSRDM’s two key modeling contributions (multi-level recurrent feedback and system-level switches) improve forecasts.

Fig. 3 shows sampled forecasts from our model and base-

Table 2: Statistics on NBA player forecasts.

	% In Bounds	Directional Variation
HSRDM (ours)	.915	.506
No system state (ϵ ARHMM)	.908 (.003)	.631 \times (.010)
No recurrent feedback	.814 \times (.007)	.469 (.016)

lines. We see that system-level switches help to coordinate entities; players move in more coherent directions under HSRDM than without the top-level system-state. We also see that multi-level recurrent feedback supports *location-dependent* state transitions; players are more likely to move towards feasible (in-bounds) locations under HSRDM than without recurrence. These observations are corroborated in Tab. 2, which summarizes two statistics computed over the entire test set: *% In Bounds*, the mean percentage of each forecast that is in bounds, and *Directional Variation*, which measures incoherent movements by basketball players via the circular variance across players of the movement direction between the first and last timesteps in the forecasting window. We test hypotheses as in Tab. 1. Methods significantly different from the HSRDM baseline at the .01 level are marked with a red x. We find that removing recurrence significantly reduces the mean percentage of forecasts that is in bounds, and removing the system-level switches significantly increases the directional variation across players.

5.3 Maintaining visual security in a simulated battle

As a final demonstration, we investigate the ability of a squad of active-duty soldiers in a NATO-affiliated army to maintain visual security while engaged in a simulated training exercise in which enemy fire comes from the south. Focus on the south creates a potential blindside to the north. If this blindside is left unchecked for a sufficiently long time, then at least one soldier should briefly turn their head to regain visibility and reduce the squad’s vulnerability to a blindside attack. The squad was instructed that visual security was a key subtask among several overall goals. Strong performance at this subtask requires coordination across all soldiers in the squad.

The dataset consists of soldier-specific univariate time series of heading direction angles $x_t^{(j)}$ recorded at 130 Hz from helmet inertial measurement units (IMU). We downsample to 6.5 Hz to reduce autocorrelations. We investigate a 12 minute recording of one squad of 8 soldiers. The raw data from the first minute of contact is illustrated in Fig. 4. Due to privacy concerns, data is not shareable. This study was approved by the U.S. Army Combat Capabilities Development Command Armaments Center Institutional Review Board and the Army Human Research Protections Office (Protocol Number: 18-003)

We fit our HSRDM to this data, capturing the goal of visual security by setting the system-level recurrence function g to the normalized elapsed time since any one of the J soldiers looked within the north quadrant of the circle. Soldier headings must remain on the unit circle throughout time, so we

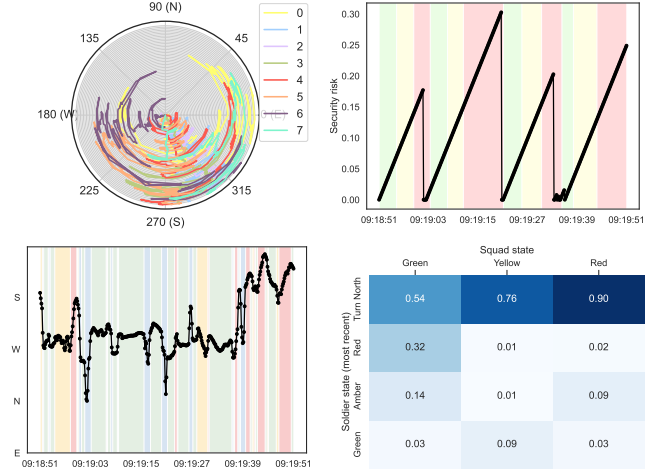


Figure 4: Modeling the heading directions of a squad of soldiers engaged in simulated battle. **Top left:** Heading directions (in degrees) of a squad of soldiers over time. Each color represents a different soldier. Time moves from center of circle to boundary. **Top right:** Inferred squad-level states $s_{0:T}$ (colors) superimposed over black curve representing the squad’s cumulative security risk in the north direction (elapsed time since any soldier checked their blindside) as a function of time. The learned red squad state seems to indicate high security risk. These squad states can modulate soldier-level heading dynamics. **Bottom left:** Inferred entity-level states $z_{0:T}$ (colors) for Soldier 6, superimposed on observed time series of heading direction from that soldier’s helmet IMU. The light blue state’s autoregressive emission dynamics produce a rapid turn to the north. Twice this state persisted long enough for the soldier to reduce security risk in the north (around 19:03 and 19:20). **Bottom right:** The learned probability that Soldier 6 turns to the north from various soldier-specific states (z , rows) depends upon the squad-level states (s , columns). The soldier is most likely to persist in turning north when the squad has a security vulnerability (s is red).

use *Von Mises autoregressions* as the emission model H_C for the k -th state of the j -th soldier:

$$x_t^{(j)} \mid x_{t-1}^{(j)}, \{z_t^{(j)}=k\} \sim \mathcal{VM}(\mu_{j,k}(x_{t-1}^{(j)}), \kappa_{j,k}),$$

$$\text{where } \mu_{j,k}(x_{t-1}^{(j)}) = \alpha_{j,k} x_{t-1}^{(j)} + \delta_{j,k} \quad (5.1)$$

The Von Mises distribution [Banerjee et al., 2005, Fisher and Lee, 1994], denoted $\mathcal{VM}(\mu, \kappa)$, is a distribution over angles on the unit circle, governed by mean μ and concentration $\kappa > 0$. Here, $\alpha_{j,k}$ is an autoregressive coefficient, $\delta_{j,k}$ is a drift term, and $\kappa_{j,k}$ is a concentration for entity j in state k .

Using the inference method from Sec. 3, we obtained the results visualized in Fig. 4. Inspection of the inferred system-level states, entity-level states, and learned transition probabilities suggests that the model learns a special turn north state (blue) for Soldier 6 that is particularly probable when

the entire squad reaches the red state of high elapsed time since any blindside check.

6 Conclusion

We have introduced a family of models for capturing the dynamics of individual entities evolving in coordinated fashion within a shared environment over the same time period. These models admit efficient structured variational inference in which coordinate ascent can alternate between E-step dynamic programming routines similar to classic forward-backward recursions to infer hidden state posteriors at both system- and entity-levels and M-step updates to transition and emission parameters that also use closed-form updates when possible. Across several datasets, we’ve shown our approach represents a natural way to capture system-to-entity and entity-to-system coordination while keeping costs linear in the number of entities.

Limitations. Several coordinate ascent steps in any per-entity rAR-HMM with Gaussian emissions scale quadratically in D , so scaling beyond a few dozen features presents a challenge. Furthermore, the parametric forms of both transitions and emissions in our model allow tractability but clearly limit expressivity compared to recent deep probabilistic models [Krishnan et al., 2017]. Scaling to many more entities would require extensions of our structured VI to process minibatches of entities [Hoffman et al., 2013]. Scaling to much longer sequences might require processing randomly sampled windows [Foti et al., 2014].

Future directions. For some applied tasks, it may be promising to extend our two-level system-entity hierarchy to even more levels (e.g. to represent nested structures of platoons, squads, and individual soldiers all pursuing the same mission). Additionally, we could extend from rARHMMs to switching linear dynamical systems by adding an additional latent continuous variable sequence between discretized z and observations x in the graphical model.

Acknowledgments

This research was sponsored by the U.S. Army DEVCOM Soldier Center, and was accomplished under Cooperative Agreement Number W911QY-19-2-0003. The views and conclusions contained in this document are those of the authors and should not be interpreted as representing the official policies, either expressed or implied, of the U.S. Army DEVCOM Soldier Center, or the U.S. Government. The U. S. Government is authorized to reproduce and distribute reprints for Government purposes notwithstanding any copyright notation hereon.

Approved for Public Release OPSEC # PR2023_28848

References

- Alaa, A. M. and van der Schaar, M. (2019). Attentive state-space modeling of disease progression. *Advances in neural information processing systems*, 32.

- Alameda-Pineda, X., Drouard, V., and Horaud, R. P. (2021). Variational inference and learning of piecewise linear dynamical systems. *IEEE Transactions on Neural Networks and Learning Systems*, 33(8):3753–3764.
- Alcorn, M. A. and Nguyen, A. (2021). *Baller2vec++: A Look-Ahead Multi-Entity Transformer For Modeling Coordinated Agents*.
- Altman, R. M. (2007). Mixed hidden markov models: an extension of the hidden markov model to the longitudinal data setting. *Journal of the American Statistical Association*, 102(477):201–210.
- Ansari, A. F., Benidis, K., Kurle, R., Türkmen, A. C., Soh, H., Smola, A. J., Wang, Y., and Januschowski, T. (2021). Deep Explicit Duration Switching Models for Time Series. In *Advances in Neural Information Processing Systems (NeurIPS)*.
- Banerjee, A., Dhillon, I. S., Ghosh, J., Sra, S., and Ridgeway, G. (2005). Clustering on the unit hypersphere using von mises-fisher distributions. *Journal of Machine Learning Research*, 6(9).
- Barber, D., Cemgil, A. T., and Chiappa, S. (2011). *Bayesian time series models*. Cambridge University Press.
- Beal, M. J. (2003). *Variational algorithms for approximate Bayesian inference*. University of London, University College London (United Kingdom).
- Benjamini, Y. and Hochberg, Y. (1995). Controlling the false discovery rate: a practical and powerful approach to multiple testing. *Journal of the Royal statistical society: series B (Methodological)*, 57(1):289–300.
- Blei, D. M., Kucukelbir, A., and McAuliffe, J. D. (2017). Variational inference: A review for statisticians. *Journal of the American statistical Association*, 112(518):859–877.
- Bradbury, J., Frostig, R., Hawkins, P., Johnson, M. J., Leary, C., Maclaurin, D., Necula, G., Paszke, A., VanderPlas, J., Wanderman-Milne, S., and Zhang, Q. (2018). JAX: Composable transformations of Python+NumPy programs.
- Bui, H. H., Phung, D. Q., and Venkatesh, S. (2004). Hierarchical Hidden Markov Models with General State Hierarchy. In *Proceedings of the National Conference on Artificial Intelligence (AAAI)*.
- Dong, Z., Seybold, B. A., Murphy, K. P., and Bui, H. H. (2020). Collapsed amortized variational inference for switching nonlinear dynamical systems. In *International Conference on Machine Learning*.
- Farnoosh, A., Azari, B., and Ostadabbas, S. (2021). Deep Switching Auto-Regressive Factorization: Application to Time Series Forecasting. In *AAAI Conference on Artificial Intelligence*.
- Felsen, P., Lucey, P., and Ganguly, S. (2018). Where will they go? predicting fine-grained adversarial multi-agent

- motion using conditional variational autoencoders. In *Proceedings of the European conference on computer vision (ECCV)*, pages 732–747.
- Fine, S., Singer, Y., and Tishby, N. (1998). The Hierarchical Hidden Markov Model: Analysis and Applications. *Machine Learning*, 32.
- Fisher, N. and Lee, A. (1994). Time series analysis of circular data. *Journal of the Royal Statistical Society: Series B (Methodological)*, 56(2):327–339.
- Foti, N., Xu, J., Laird, D., and Fox, E. (2014). Stochastic variational inference for hidden Markov models. In *Advances in Neural Information Processing Systems*.
- Fox, E. B., Hughes, M. C., Sudderth, E. B., and Jordan, M. I. (2014). Joint modeling of multiple time series via the beta process with application to motion capture segmentation. *Annals of Applied Statistics*, 8(3):1281–1313.
- Fox, E. B., Sudderth, E. B., Jordan, M. I., and Willsky, A. S. (2011). A sticky HDP-HMM with application to speaker diarization. *Annals of Applied Statistics*, 5(2A):1020–1056.
- Ghahramani, Z. and Hinton, G. E. (2000). Variational learning for switching state-space models. *Neural computation*, 12(4):831–864.
- Gu, A., Goel, K., and Ré, C. (2022). Efficiently Modeling Long Sequences with Structured State Spaces. In *International Conference on Learning Representations (ICLR)*. arXiv.
- Hamilton, J. D. (1994). *Time series analysis*. Princeton university press.
- Hamilton, J. D. (2010). Regime switching models. *Macroeconomics and time series analysis*, pages 202–209.
- Hamilton, J. D. (2020). *Time series analysis*. Princeton university press.
- Heller, K. A., Teh, Y. W., and Görür, D. (2009). Infinite hierarchical hidden Markov models. In *Artificial Intelligence and Statistics*.
- Hoffman, M., Blei, D., Wang, C., and Paisley, J. (2013). Stochastic Variational Inference. *Journal of Machine Learning Research*, 14(1).
- Kipf, T., Fetaya, E., Wang, K.-C., Welling, M., and Zemel, R. (2018). Neural Relational Inference for Interacting Systems. In *Proceedings of the 35th International Conference on Machine Learning*, pages 2688–2697. PMLR.
- Krishnan, R. G., Shalit, U., and Sontag, D. (2017). Structured Inference Networks for Nonlinear State Space Models. In *AAAI Conference on Artificial Intelligence*. arXiv.
- Linderman, S., Johnson, M., Miller, A., Adams, R., Blei, D., and Paninski, L. (2017). Bayesian learning and inference in recurrent switching linear dynamical systems. In *Artificial Intelligence and Statistics*, pages 914–922. PMLR.
- Linderman, S., Nichols, A., Blei, D., Zimmer, M., and Paninski, L. (2019). Hierarchical recurrent state space models reveal discrete and continuous dynamics of neural activity in *C. elegans*.
- Linou, K. (2016). NBA Player Movements.
- Liu, D., Lu, T., Niu, X.-F., and Wu, H. (2011). Mixed-effects state-space models for analysis of longitudinal dynamic systems. *Biometrics*, 67(2):476–485.
- Lucey, P., Bialkowski, A., Carr, P., Morgan, S., Matthews, I., and Sheikh, Y. (2013). Representing and discovering adversarial team behaviors using player roles. In *Proceedings of the IEEE Conference on Computer Vision and Pattern Recognition*, pages 2706–2713.
- Metulini, R., Manisera, M., and Zuccolotto, P. (2018). Modelling the dynamic pattern of surface area in basketball and its effects on team performance. *Journal of Quantitative Analysis in Sports*, 14(3):117–130.
- Miller, A. C. and Bornn, L. (2017). Possession Sketches: Mapping NBA Strategies. In *MIT Sloan Sports Analytics Conference*.
- Nassar, J., Linderman, S. W., Bugallo, M., and Park, I. M. (2019). Tree-Structured Recurrent Switching Linear Dynamical Systems for Multi-Scale Modeling. In *International Conference on Learning Representations*. arXiv.
- Nguyen, N., Phung, D., Venkatesh, S., and Bui, H. (2005). Learning and detecting activities from movement trajectories using the hierarchical hidden Markov model. In *2005 IEEE Computer Society Conference on Computer Vision and Pattern Recognition (CVPR’05)*, volume 2, pages 955–960 vol. 2.
- Raabe, D., Nabben, R., and Memmert, D. (2023). Graph representations for the analysis of multi-agent spatiotemporal sports data. *Applied Intelligence*, 53(4):3783–3803.
- Rabiner, L. R. (1989). A Tutorial on Hidden Markov Models and Selected Applications in Speech Recognition. *Proc. of the IEEE*, 77(2):257–286.
- Rangapuram, S. S., Seeger, M., Gasthaus, J., Stella, L., Wang, Y., and Januschowski, T. (2018). Deep State Space Models for Time Series Forecasting. In *Advances in Neural Information Processing Systems (NeurIPS)*.
- Sanchez-Gonzalez, A., Godwin, J., Pfaff, T., Ying, R., Leskovec, J., and Battaglia, P. (2020). Learning to Simulate Complex Physics with Graph Networks. In *Proceedings of the 37th International Conference on Machine Learning*, pages 8459–8468. PMLR.
- Severson, K. A., Chahine, L. M., Smolensky, L., Ng, K., Hu, J., and Ghosh, S. (2020). Personalized input-output hidden markov models for disease progression modeling. In *Machine Learning for Healthcare Conference*, pages 309–330. PMLR.
- Shumway, R. H. and Stoffer, D. S. (1982). An Approach to Time Series Smoothing and Forecasting Using the Em

- Algorithm. *Journal of Time Series Analysis*, 3(4):253–264.
- Shumway, R. H., Stoffer, D. S., and Stoffer, D. S. (2000). *Time series analysis and its applications*, volume 3. Springer.
- Skounakis, M., Craven, M., and Ray, S. (2003). Hierarchical Hidden Markov Models for Information Extraction. In *International Joint Conferences on Artificial Intelligence (IJCAI)*.
- Stanculescu, I., Williams, C. K. I., and Freer, Y. (2014). A Hierarchical Switching Linear Dynamical System Applied to the Detection of Sepsis in Neonatal Condition Monitoring. In *Uncertainty in Artificial Intelligence*.
- Sun, J. J., Karigo, T., Chakraborty, D., Mohanty, S. P., Wild, B., Sun, Q., Chen, C., Anderson, D. J., Perona, P., Yue, Y., and Kennedy, A. (2021). The Multi-Agent Behavior Dataset: Mouse Dyadic Social Interactions.
- Terner, Z. and Franks, A. (2021). Modeling Player and Team Performance in Basketball. *Annual Review of Statistics and Its Application*, 8(1):1–23.
- van Dijk, D., Teräsvirta, T., and Franses, P. H. (2002). Smooth Transition Autoregressive Models — a Survey of Recent Developments. *Econometric Reviews*, 21(1):1–47.
- Wojnowicz, M., Buck, M. D., and Hughes, M. C. (2023). Approximate inference by broadening the support of the likelihood. In *Fifth Symposium on Advances in Approximate Bayesian Inference*.
- Xu, C., Li, M., Ni, Z., Zhang, Y., and Chen, S. (2022). GroupNet: Multiscale hypergraph neural networks for trajectory prediction with relational reasoning. In *Proceedings of the IEEE/CVF Conference on Computer Vision and Pattern Recognition*.
- Xu, X. and Chen, Y. (2021). Deep Switching State Space Model (DSS³M) for Nonlinear Time Series Forecasting with Regime Switching.
- Yeh, R. A., Schwing, A. G., Huang, J., and Murphy, K. (2019). Diverse generation for multi-agent sports games. In *Proceedings of the IEEE/CVF Conference on Computer Vision and Pattern Recognition*, pages 4610–4619.
- Yuan, Y., Weng, X., Ou, Y., and Kitani, K. M. (2021). AgentFormer: Agent-Aware Transformers for Socio-Temporal Multi-Agent Forecasting. In *Proceedings of the IEEE/CVF International Conference on Computer Vision*, pages 9813–9823.
- Zhan, E., Zheng, S., Yue, Y., Sha, L., and Lucey, P. (2019). Generating Multi-Agent Trajectories using Programmatic Weak Supervision. In *International Conference on Learning Representations*.

Supplementary Appendix

Contents of Supplementary Appendix

A	Recurrent Autoregressive HMMs: Model and Inference Details	13
A.1	Model	13
A.2	State Estimation	14
A.3	Entropy	17
B	Proposed HSRDM: Model and Inference Details	17
B.1	Priors on model parameters	18
B.2	Updating the posterior over system-level states	18
B.3	Updating the posterior over entity-level states	19
B.4	Updating the parameters	19
B.5	Variational lower bound	20
B.6	Smart initialization	20
B.7	Multiple Examples	21
C	Methodology: Supplemental Information	22
C.1	Model fit	22
C.2	Partial forecasting	22
D	FigureEight Toy Data: Supplemental Information	23
D.1	Data generating process	23
D.2	Dataset	24
D.3	Methods	24
D.4	Results	24
E	Visual Security Experiment: Supplemental Information	28
F	Basketball Experiment: Supplemental Information	28
F.1	Dataset	28
F.2	Evaluation strategy	30
F.3	Models	31
F.4	Future directions	32
G	Code	33

A Recurrent Autoregressive HMMs: Model and Inference Details

As detailed below in Sec. A.1, a recurrent autoregressive Hidden Markov Model ($rARHMM$) generalizes a standard Hidden Markov Model by adding autoregressive and recurrent edges to the probabilistic graphical model. Although $rARHMM$ models have been previously proposed in the literature [Linderman et al., 2017], we do not know of any explicit proposition (or justification) describing how to perform posterior state inference for these models. The literature provides such a proposition for (non-recurrent) autoregressive Hidden Markov Model ($ARHMM$ s; e.g., see [Hamilton, 2020]), but not for $rARHMM$ s. Hence, we provide the missing propositions with proofs here; see Props. A.2.1 and A.2.2. We believe that these explicit propositions can be useful when composing recurrence into more complicated constructions. Indeed, we use them throughout the supplement in order to derive inference for our $HSRDMS$ s; for example, see the VES step in Sec. B.2 or the VEZ step in Sec. B.3. In fact, we also utilize the proofs of these propositions when describing how to perform inference with $HSRDMS$ s when the dataset is partitioned into multiple examples; see Sec. B.7.

A.1 Model

The complete data likelihood for a (K, m, n) -order recurrent AR-HMM ($rARHMM$) is given by Radon-Nikodým density

$$p(\mathbf{x}_{1:T}, \mathbf{z}_{1:T} | \theta) = \underbrace{p(z_1 | \theta)p(\mathbf{x}_1 | z_1, \theta)}_{\text{initialization}} \prod_{t=2}^T \underbrace{p(z_t | z_{t-1}, \mathbf{x}_{(t-m):(t-1)}, \theta)}_{\text{transitions}} \underbrace{p(\mathbf{x}_t | z_t, \mathbf{x}_{(t-n):(t-1)}, \theta)}_{\text{emissions}} \quad (\text{A.1})$$

where $\mathbf{x}_{1:T}$ are the observations, $\mathbf{z}_{1:T} \in \{1, \dots, K\}$ are the discrete latent states, and θ are the parameters. The $rARHMM$ generalizes the standard HMM [Rabiner, 1989], which contains neither autoregressive emissions (blue) nor recurrent feedback (red) from emissions to states. The (K, m, n) -order $rARHMM$ gives a (K, n) -order autoregressive HMM ($ARHMM$) in the special case where

$$p(z_t | z_{t-1}, \mathbf{x}_{(t-m):(t-1)}, \theta) = p(z_t | z_{t-1}, \theta) \quad (\text{A.2})$$

See Fig. A.1 for a probabilistic graphical model representation in the special case of first-order recurrence ($m = 1$) and autoregression ($n = 1$).

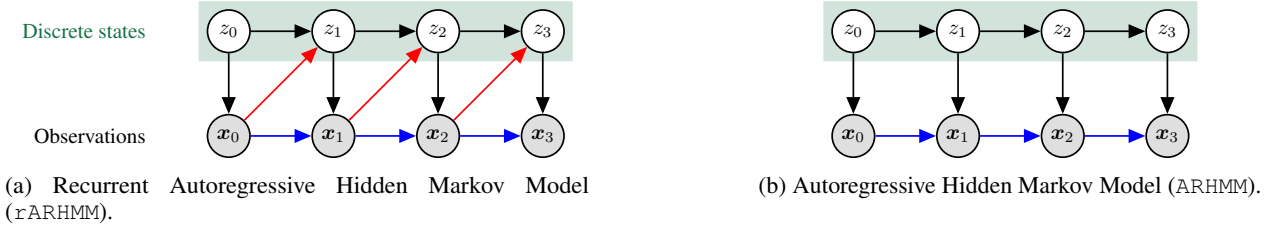


Figure A.1: Probabilistic graphical model representation of a Recurrent Autoregressive HMM ($rARHMM$), and its special case, an Autoregressive HMM ($ARHMM$). For simplicity the illustration assumes first-order autoregression and recurrence, but higher-order dependencies can also be accommodated (see Eq. (A.1) and Props. A.2.1 and A.2.2). Autoregressive edges are shown in blue and recurrent edges are shown in red.

Remark A.1.1. (On generalizing a HMM with autoregressive emissions and recurrent state transitions.) Let us highlight how a $rARHMM$ model generalizes a conventional HMM:

- *Recurrence:* A lookback window of n previous observations $\mathbf{x}_{t-n:t-1}$ can influence the transitions structure for the current state z_t .

$$\mathbf{pa}(z_t) = \{z_{t-1}\} \cup \underbrace{\{\mathbf{x}_{(t-n):(t-1)}\}}_{\text{if recurrent}}$$

- *Autoregression:* A lookback window of m previous observations $\mathbf{x}_{t-m:t-1}$ can influence the emissions structure for the current observation x_t .

$$\mathbf{pa}(x_t) = \{z_t\} \cup \underbrace{\{\mathbf{x}_{(t-m):(t-1)}\}}_{\text{if autoregressive}}$$

Note in particular that each node (observation x_t or state z_t) can have *many* parents among previous observation variables $\mathbf{x}_{1:t}$, but only *one* parent among state variables $\mathbf{z}_{1:t}$ (namely, the closest in time from the present or past).¹ This assumption will be important when deriving the smoother in Sec. A.2. \triangle

¹What if we wanted to relax the specification so that the emissions could depend on a finite number M of previous states

A.2 State Estimation

Here we discuss state estimation for the r ARHMM. We begin with some notation.

Notation A.2.1. Given a sequence of observations up to some time t , we can define the conditional probability of the state z_s at a target time $s \in \{1, 2, \dots, T\}$ via the probability vector $\xi_{s|t} \in \Delta_{K-1} \subset \mathbb{R}^K$. The k -th element of this vector is given by $p_\theta(z_s = k | \mathbf{x}_{1:t})$. That is,

$$\xi_{s|t} \triangleq p_\theta(z_s | \mathbf{x}_{1:t}) = \left[p_\theta(z_s = 1 | \mathbf{x}_{1:t}), \dots, p_\theta(z_s = K | \mathbf{x}_{1:t}) \right]^T$$

Using this notation, we can define three common inferential tasks:

1. *Filtering.* Infer the current state given observations $\xi_t | t = p_\theta(z_t | \mathbf{x}_{1:t})$.
2. *Smoothing.* Infer a past state given observations $\xi_s | t = p_\theta(z_s | \mathbf{x}_{1:t})$, where $s < t$.
3. *Prediction.* Predict a future state given observations, $\xi_u | t = p_\theta(z_u | \mathbf{x}_{1:t})$, where $u > t$.

△

Now we can give Props. A.2.1 and A.2.2, which parallel the presentation of the Kalman filter and smoother in the context of state space models [Hamilton, 2020, Shumway et al., 2000]. In particular, we will present the forward algorithm in terms of a *measurement update* (which uses the observation \mathbf{x}_t to transform $\xi_{t|t-1}$ into $\xi_t | t$) and a *time update* (which transforms $\xi_t | t$ into $\xi_{t+1|t}$, without requiring an observation). These propositions show that *filtering* and *smoothing* can be done using the same recursions as used in a classical HMM [Hamilton, 1994], except that the variable interpretations differ for both the emissions step and transition step. In the statements and proofs below, we continue to use the same color scheme as was used in Eq. (A.1) and Fig. A.1, whereby blue designates autoregressive edges and red designates recurrence edges in the graphical model. These colors highlight differences from classic HMMs, which lack both types of edges.

Proposition A.2.1. (Filtering a Recurrent Autoregressive HMM.) Filtered probabilities $\xi_t | t \triangleq p_\theta(z_t | \mathbf{x}_{1:t})$ for a Recurrent Autoregressive Hidden Markov Model can be obtained by recursively updating some initialization $\xi_{1|0}$ by

- Measurement update.

$$\xi_t | t = \frac{(\xi_{t|t-1} \odot \epsilon_t)}{\mathbf{1}^T (\xi_{t|t-1} \odot \epsilon_t)}$$

- Time update.

$$\xi_{t+1|t} = \mathbf{A}_t \xi_t | t$$

where here $\epsilon_t = (\epsilon_{t1}, \dots, \epsilon_{tk}) = (p_\theta(\mathbf{x}_t | z_t = k, \mathbf{x}_{1:t-1}))_{k=1}^K$ is the $(K \times 1)$ vector whose k -th element is the emissions density, \mathbf{A}_t represents the $(K \times K)$ transition matrix whose (k, k') -th element is $p_\theta(z_{t+1} = k' | z_t = k, \mathbf{x}_{1:t})$, $\mathbf{1}$ represents a $(K \times 1)$ vector of 1s, and the symbol \odot denotes element-by-element multiplication.

Proof.

- Measurement update.

$$\begin{aligned} \xi_t | t &= p_\theta(z_t | \mathbf{x}_{1:t}) && \text{Notation} \\ &\propto p_\theta(z_t, \mathbf{x}_t | \mathbf{x}_{1:t-1}) && \text{Conditional density} \\ &= \underbrace{p_\theta(z_t | \mathbf{x}_{1:t-1})}_{\triangleq \xi_{t|t-1}} \odot \underbrace{p_\theta(\mathbf{x}_t | z_t, \mathbf{x}_{1:t-1})}_{\triangleq \epsilon_t} && \text{Chain rule} \\ \implies \xi_t | t &= \frac{(\xi_{t|t-1} \odot \epsilon_t)}{\mathbf{1}^T (\xi_{t|t-1} \odot \epsilon_t)} && \text{Normalize} \end{aligned}$$

$p(\mathbf{x}_t | z_t, z_{t-1}, \dots, z_{t-M}, \mathbf{x}_{1:t-1}, \phi)$? This situation can be handled by simply redefining the states in terms of tuples $z_t^* = (z_t, z_{t-1}, \dots, z_{t-M})$, such that z_t^* takes on K^M possible values, one for each sequence in the look-back window [Hamilton, 2010, pp.8].

- Time update.

$$\begin{aligned}
 \xi_{t+1|t} &= p_\theta(z_{t+1} | \mathbf{x}_{1:t}) && \text{Def.} \\
 &= \sum_{k=1}^K p_\theta(z_{t+1}, z_t = k | \mathbf{x}_{1:t}) && \text{Law of Total Prob.} \\
 &= \sum_{k=1}^K p_\theta(z_{t+1} | z_t = k, \mathbf{x}_{1:t}) p_\theta(z_t = k | \mathbf{x}_{1:t}) && \text{Chain rule} \\
 &= \sum_{k=1}^K \underbrace{\left[\mathbf{A}_t \right]_{k,:}}_{\text{kth row of } \mathbf{A}_t} \underbrace{\left[\xi_{t|t} \right]_k}_{\text{kth element of } \xi_{t|t}} && \text{Notation} \\
 &= \mathbf{A}_t \xi_{t|t} && \text{Def. matrix multiplication}
 \end{aligned}$$

□

Remark A.2.1. (*Initializing the filtering algorithm in Prop. A.2.1.*) Inspired by Hamilton [1994, pp.693], we provide some suggestions for initializing the filtering algorithm of Prop A.2.1. In particular, we can set $\xi_{1|0}$ to

- Any reasonable probability vector, such as the uniform distribution $K^{-1}\mathbf{1}$.
- The maximum likelihood estimate.
- The steady state transition probabilities, if they exist.

△

Proposition A.2.2. (Smoothing a Recurrent Autoregressive Hidden Markov Model.) Smoothed probabilities $\xi_{t|T} \triangleq p_\theta(z_t | \mathbf{x}_{1:T})$ for a Hidden Markov Model can be obtained by the recursion

$$\xi_{t|T} = \xi_{t|t} \odot \left\{ \mathbf{A}_t^T \cdot \left[\xi_{t+1|T} (\div) \xi_{t+1|t} \right] \right\}$$

where the formula is initialized by $\xi_{T|T}$ (obtained from the filtering algorithm of Prop. A.2.1) and is then iterated backwards for $t = T-1, T-2, \dots, 1$, in a step analogous to the backward pass of the classic forward-backward recursions for plain HMMs [Rabiner, 1989]. Here, \mathbf{A}_t represents the $(K \times K)$ transition matrix whose (k, k') -th element is $p_\theta(z_{t+1} = k' | z_t = k, \mathbf{x}_{1:t})$, the symbol \odot denotes element-wise multiplication, and the symbol (\div) denotes element-wise division.

*Proof.*²

We proceed in steps:

- **Step 1** We show $p_\theta(z_t | z_{t+1}, \mathbf{x}_{1:T}) = p_\theta(z_t | z_{t+1}, \mathbf{x}_{1:t})$. That is, the current state z_t depends on future observations $\mathbf{x}_{t+1:T}$ only through the next state z_{t+1} .

– **Step 1a** We show $p_\theta(z_t | z_{t+1}, \mathbf{x}_{1:t+1}) = p_\theta(z_t | z_{t+1}, \mathbf{x}_{1:t})$.

$$\begin{aligned}
 p_\theta(z_t | z_{t+1}, \mathbf{x}_{1:t+1}) &= p_\theta(z_t | z_{t+1}, \mathbf{x}_{t+1}, \mathbf{x}_{1:t}) && \text{split off term from sequence} \\
 &= \frac{p_\theta(z_t, \mathbf{x}_{t+1} | z_{t+1}, \mathbf{x}_{1:t})}{p_\theta(\mathbf{x}_{t+1} | z_{t+1}, \mathbf{x}_{1:t})} && \text{conditional density} \\
 &= \frac{p_\theta(\mathbf{x}_{t+1} | z_t, z_{t+1}, \mathbf{x}_{1:t}) p_\theta(z_t | z_{t+1}, \mathbf{x}_{1:t})}{p_\theta(\mathbf{x}_{t+1} | z_{t+1}, \mathbf{x}_{1:t})} && \text{chain rule} \\
 &= p_\theta(z_t | z_{t+1}, \mathbf{x}_{1:t}) && \text{FPOBN}
 \end{aligned}$$

In the last line, the two canceled terms are equal by FPOBN (the Fundamental Property of Bayes Networks).³

²Our proof is inspired by the proof given by Hamilton [1994, pp.700-702] for the ARHMM (i.e, the special case of rARHMM in which there are no recurrent edges).

³The Fundamental Property of Bayes Networks is: *A node is independent of its non-descendants given its parents.* In particular, since z_t is a non-descendent of \mathbf{x}_{t+1} , it is independent of \mathbf{x}_{t+1} given its parents z_{t+1} and $\mathbf{x}_{1:t}$.

- **Step 1b** We show $p_\theta(z_t | z_{t+1}, \mathbf{x}_{1:t+2}) = p_\theta(z_t | z_{t+1}, \mathbf{x}_{1:t+1})$. By the same argument as in step 1a (splitting up the sequence, conditional density, chain rule), but replacing

$$\mathbf{x}_{1:t+1} \leftarrow \mathbf{x}_{1:t+2} \quad , \quad \mathbf{x}_{t+1} \leftarrow \mathbf{x}_{t+2}$$

the proposition holds if

$$p(\mathbf{x}_{t+2} | z_t, z_{t+1}, \mathbf{x}_{1:t+1}) = p(\mathbf{x}_{t+2} | z_{t+1}, \mathbf{x}_{1:t+1})$$

that is if we get the same cancelation. And we see

$$\begin{aligned} p(\mathbf{x}_{t+2} | z_t, z_{t+1}, \mathbf{x}_{1:t+1}) &= \sum_{k=1}^K p(\mathbf{x}_{t+2}, z_{t+2} = k | z_t, z_{t+1}, \mathbf{x}_{1:t+1}) && \text{LTP} \\ &= \sum_{k=1}^K p(\mathbf{x}_{t+2} | z_{t+2} = k, z_t, z_{t+1}, \mathbf{x}_{1:t+1}) p(z_{t+2} = k | z_t, z_{t+1}, \mathbf{x}_{1:t+1}) && \text{chain rule, FPOBN} \\ &= \sum_{k=1}^K p(\mathbf{x}_{t+2}, z_{t+2} = k | z_{t+1}, \mathbf{x}_{1:t+1}) && \text{undo chain rule} \\ &= p(\mathbf{x}_{t+2} | z_{t+1}, \mathbf{x}_{1:t+1}) && \text{undo LTP} \end{aligned}$$

- **Conclusion** The claim follows from Steps 1a and 1b by an induction argument.

- **Step 2.** We show that
$$\underbrace{p(z_t, z_{t+1} | \mathbf{x}_{1:T})}_{\text{smoothed pairwise}} = \underbrace{p(z_{t+1} | \mathbf{x}_{1:T})}_{\text{smoothed}} \underbrace{p(z_{t+1} | z_t, \mathbf{x}_{1:t})}_{\text{transition}} \underbrace{\frac{p(z_t | \mathbf{x}_{1:t})}{p(z_{t+1} | \mathbf{x}_{1:t})}}_{\text{filtered predicted}}.$$
 We have

$$\begin{aligned} p(z_t, z_{t+1} | \mathbf{x}_{1:T}) &= p(z_{t+1} | \mathbf{x}_{1:T}) p(z_t | z_{t+1}, \mathbf{x}_{1:T}) && \text{chain rule} \\ &= p(z_{t+1} | \mathbf{x}_{1:T}) p(z_t | z_{t+1}, \mathbf{x}_{1:t}) && \text{Step 1} \\ &= p(z_{t+1} | \mathbf{x}_{1:T}) \frac{p(z_t | \mathbf{x}_{1:t}) p(z_{t+1} | z_t, \mathbf{x}_{1:t})}{p(z_{t+1} | \mathbf{x}_{1:t})} && \text{Bayes rule (on 2nd term)}^4 \end{aligned}$$

- **Step 3.** We prove the proposition.

$$\begin{aligned} p(z_t | \mathbf{x}_{1:T}) &= \sum_{k=1}^K p(z_t, z_{t+1} = k | \mathbf{x}_{1:T}) && \text{Law of Total Prob.} \\ \xi_t | T &= \sum_{k=1}^K \left[\xi_{t+1} | T \right]_k \left[\mathbf{A}_t \right]_{:, z_{t+1}=k} \frac{\xi_t | t}{\left[\xi_{t+1} | t \right]_k} && \text{Step 2, Notation} \\ &= \xi_t | t \sum_{k=1}^K \left[\mathbf{A}_t \right]_{:, z_{t+1}=k} \frac{\left[\xi_{t+1} | T \right]_k}{\left[\xi_{t+1} | t \right]_k} && \text{Pull out constant} \\ &= \xi_t | t \odot \left\{ \mathbf{A}_t^T \cdot \left[\xi_{t+1} | T \right] (\div) \xi_{t+1} | t \right\} && \text{Def. matrix multiplication} \end{aligned}$$

□

Remark A.2.2. As we saw in Step 1, the derivation of the smoother in Prop. A.2.2 relies on the fact that while each node (observation or state) can have *many* observation parents, it can have only *one* state parent (namely, the closest in time from the present or past). \triangle

⁴To justify the application of Bayes rule, imagine that z_t plays the role of the parameter and z_{t+1} plays the role of the observed data. The term $\mathbf{x}_{1:t}$ is just a conditioning set throughout.

Remark A.2.3. The filtering (Prop A.2.1) and smoothing (Prop A.2.2) formulae reveal that state estimation for rARHMM can be handled for :

- any order of recurrence and/or autoregression⁵
- any functional form of emissions and transitions

Furthermore, although it was not explicitly represented here, the same formulae hold when there are

- Modulation of transitions and emissions by *exogenous covariates*.⁶

△

A.3 Entropy

Here, we provide the entropy of an rARHMM posterior. We write the complete data likelihood of Eq. (A.1) as $p_\theta(\mathbf{x}_{1:T}, \mathbf{z}_{1:T})$. Then the posterior distribution (of the states $\mathbf{z}_{1:T}$ given the observations $\mathbf{x}_{1:T}$) is

$$p_\theta(\mathbf{z}_{1:T} | \mathbf{x}_{1:T}) = \frac{p_\theta(\mathbf{x}_{1:T}, \mathbf{z}_{1:T})}{\underbrace{p_\theta(\mathbf{x}_{1:T})}_{\triangleq Z_\theta}} \quad (\text{A.3})$$

where $Z_\theta \triangleq p_\theta(\mathbf{x}_{1:T})$ is the normalizing constant (as it is constant in the states $\mathbf{z}_{1:T}$). Our interest is in computing the entropy of the posterior, $\mathbb{H}[p_\theta(\mathbf{z}_{1:T} | \mathbf{x}_{1:T})]$. We have

$$\begin{aligned} \mathbb{H}[p_\theta(\mathbf{z}_{1:T} | \mathbf{x}_{1:T})] &= - \sum_{\mathbf{k}_{1:T} \in \{1, \dots, K\}^T} p_\theta(\mathbf{z}_{1:T} = \mathbf{k}_{1:T} | \mathbf{x}_{1:T}) \log p_\theta(\mathbf{z}_{1:T} = \mathbf{k}_{1:T} | \mathbf{x}_{1:T}) && \text{def. entropy} \\ &= - \sum_{\mathbf{k}_{1:T} \in \{1, \dots, K\}^T} p_\theta(\mathbf{z}_{1:T} = \mathbf{k}_{1:T} | \mathbf{x}_{1:T}) \log p_\theta(\mathbf{z}_{1:T} = \mathbf{k}_{1:T}, \mathbf{x}_{1:T}) - \log Z_\theta && \text{by Eq. (A.3)} \\ &\stackrel{*}{=} \left[- \sum_{k=1}^K \underbrace{p_\theta(z_1 = k | \mathbf{x}_{1:T})}_{\text{posterior init}} \log \underbrace{p_\theta(z_1 = k)}_{\text{model init}} \right. \\ &\quad - \sum_{t=2}^T \sum_{k=1}^K \sum_{k'=1}^K \underbrace{p_\theta(z_t = k', z_{t-1} = k | \mathbf{x}_{1:T})}_{\text{posterior pairwise marginals}} \log \underbrace{p_\theta(z_t = k' | z_{t-1} = k, \mathbf{x}_{(t-m):(t-1)})}_{\text{model transitions}} \\ &\quad \left. - \sum_{t=1}^T \sum_{k=1}^K \underbrace{p_\theta(z_t = k | \mathbf{x}_{1:T})}_{\text{posterior unary marginals}} \log \underbrace{p_\theta(\mathbf{x}_t | z_t = k, \mathbf{x}_{(t-n):(t-1)})}_{\text{model emissions}} \right] && \text{by Eq. (A.1)} \\ &\quad - \log \underbrace{p_\theta(\mathbf{x}_{1:T})}_{\text{normalizing constant}} && \text{def } Z_\theta. \end{aligned}$$

So the entropy is given by a combination of model factors and posterior factors (recovered by smoothing). The formula in the first line of the equation above is difficult to compute, because smoothing does not directly produce a probability distribution over sequences - only over unary and pairwise marginals. However, in the Equality marked (*), we utilize the graphical structure of the model to obtain a tractable expression.

B Proposed HSRDM: Model and Inference Details

We now review modeling and inference details for our proposed HSRDM, in the following sections

- Sec. B.1 covers the prior on model parameters θ

⁵In fact, the proof reveals that the order can increase with timestep t , opening the door to constructions involving exponential weighted moving averages.

⁶A sequence of vectors $\{\mathbf{u}_t\}$ is considered to be a sequence of exogenous covariates if each \mathbf{u}_t contains no information about z_t that is not contained in $\mathbf{x}_{1:t-1}$ [Hamilton, 1994, pp.692].

- Sec. B.2 covers the VES update for system-level state posteriors
- Sec. B.3 covers the VEZ update for entity-level state posteriors
- Sec. B.4 covers the M step for transition and emission parameters
- ELBO computation and initialization are covered in subsequent sections

B.1 Priors on model parameters

The symbol θ denotes all model parameters for our HSRDM. Using the structure of our model in Eq. (2.1), we can expand θ into constituent components: $\theta = (\theta_{ss}, \theta_{es}, \theta_{ee}, \theta_{init})$, where θ_{ss} are the parameters that govern the system-level discrete state transitions, θ_{es} govern the entity-level discrete state transitions, θ_{ee} govern the entity-level emissions, and θ_{init} govern the initial distribution for states and regimes.

We define a prior over θ whose factorization structure reflects this decomposition:

$$p(\theta) = p(\theta_{ss}) p(\theta_{es}) p(\theta_{ee}) p(\theta_{init}) \quad (\text{B.1})$$

As we see in Sec. B.4, this choice of prior simplifies the M-step.

Prior on system-level state transition parameters θ_{ss} . For the system-level transition probability matrix $\mathbf{\Pi}$, a $L \times L$ matrix whose entries are all non-negative and rows sum to one, we assume a sticky Dirichlet prior [Fox et al., 2011] to encourage self-transitions so that in typical samples, one system state would persist for long segments. Concretely, for each row we set

$$\mathbf{\Pi}_{j1}, \dots, \mathbf{\Pi}_{jL} \sim \text{Dir}(\alpha, \dots, \alpha, \alpha + \kappa, \alpha, \dots, \alpha) \quad (\text{B.2})$$

where all L entries have a symmetric base value $\alpha = 1.0$, and the added value κ that impacts the self-transition entry (the (j, j) -th entry of the matrix) is set to 10.0. We then set the log transition probability $\bar{\mathbf{\Pi}}$ to the element-wise log of $\mathbf{\Pi}$.

Prior on entity-level state transition parameters θ_{es} . In our experiments, we used a non-informative prior, $p(\theta_{es}) \propto 1$. The use of a sticky Dirichlet prior, as was used with the system-level transition parameters, could be expected to produce smoother entity-level state segmentations. Currently, the entity-level segmentations are choppier than those at the system-level (e.g., compare the bottom-left and top-right subplots of Fig. 4).

Prior on emissions θ_{ee} . In our experiments, we used a non-informative prior, $p(\theta_{ee}) \propto 1$.

Prior on initial states and observations θ_{init} . For initial states at both system and entity level, we use a symmetric Dirichlet with large concentration so that all states have reasonable probability a-priori. This avoids the pathology of ML estimation that locks into only one state as a possible initial state early in inference due to poor initialization.

B.2 Updating the posterior over system-level states

In this section, we discuss the update to the posterior over system-level states; that is, the variational E-S step of Eq. (3.2). We find

$$\begin{aligned} q(s_{0:T}) &\propto \exp \left\{ \underbrace{\log \pi_s(s_0)}_{\text{init dist}} + \underbrace{\sum_{t=1}^T \log p(s_t | s_{t-1}, \mathbf{x}_{t-1}^{(1:J)}, \theta)}_{\text{transitions}} + \underbrace{\sum_{j=1}^J \sum_{t=1}^T \mathbb{E}_{q(z_0^{(j)})} \log p(z_t^{(j)} | z_{t-1}^{(j)}, \mathbf{x}_{t-1}^{(j)}, s_t, \theta)}_{\text{emissions}} \right\} \\ &= \underbrace{\pi_s(s_0)}_{\text{init state}} \underbrace{\prod_{t=1}^T p(s_t | s_{t-1}, \mathbf{x}_{t-1}^{(1:J)}, \theta)}_{\text{transitions}} \underbrace{\prod_{j=1}^J \exp \left\{ \sum_{k=1}^K \log \pi_{z_j}(z_0^{(j)} = k) q(z_0^{(j)} = k) \right\}}_{\text{initial emissions}} \\ &\quad \underbrace{\prod_{j=1}^J \prod_{t=1}^T \exp \left\{ \sum_{k, k'=1}^K \log p(z_t^{(j)} = k' | z_{t-1}^{(j)} = k, \mathbf{x}_{t-1}^{(j)}, s_t, \theta) q(z_t^{(j)} = k', z_{t-1}^{(j)} = k) \right\}}_{\text{remaining emissions}} \quad (\text{B.3}) \end{aligned}$$

This can be considered as the posterior of an input-output Hidden Markov Model with J independent autoregressive categorical emissions. The evaluation of the transition function is $\mathcal{O}(T(L^2 + LDJM_s))$, where M_s is the dimension of the system-level covariates, and where we have assumed that the evaluation of the system-level recurrence function g takes DJM_s operations, as it would if $g_\psi(\mathbf{x}_{t-1}^{(1:J)}, \mathbf{v}_{t-1}) = (\mathbf{x}_{t-1}^{(1)}, \dots, \mathbf{x}_{t-1}^{(J)}, \mathbf{v}_{t-1})^T$. The evaluation of the emissions function

is $\mathcal{O}(TJL(K^2 + KDM_e))$, where M_e is the dimension of the entity-level covariates, and where we have assumed that the evaluation of the entity-level recurrence function f takes DM_e operations, as it would if $f_\phi(\mathbf{x}_{t-1}^{(j)}, \mathbf{u}_{t-1}^{(j)}) = (\mathbf{x}_{t-1}^{(j)}, \mathbf{u}_{t-1}^{(j)})^T$. Thus, by Props. A.2.1 and A.2.2, filtering and smoothing can be computed with $\mathcal{O}(TJ[L^2 + L(K^2 + DM_s + KDM_e)])$ runtime complexity, under mild assumptions on the recurrence functions. As a result, so can the computation of the unary and adjacent pairwise marginals necessary for the VES and M steps.

B.3 Updating the posterior over entity-level states

In this section, we discuss the update to the posterior over entity-level states; that is, the variational E-Z step of Eq. (3.2). We obtain

$$q(z_{0:T}^{(1:J)}) \propto \prod_{j=1}^J \left[\underbrace{\pi_{z_j}(z_0^{(j)})}_{\text{initial state } (\in \mathbb{R}^K)} \underbrace{\prod_{t=1}^T \exp \left\{ \sum_{\ell=1}^L \log p(z_t^{(j)} \mid z_{t-1}^{(j)}, \mathbf{x}_{t-1}^{(j)}, s_t = \ell, \theta) \right\}}_{\text{transitions } (\in \mathbb{R}^{(\tilde{T}-1) \times K \times K})} \right. \\ \left. \underbrace{p(\mathbf{x}_0^{(j)} \mid z_0^{(j)}, \theta)}_{\text{initial emission } (\in \mathbb{R}^K)} \underbrace{\prod_{t=1}^T p(\mathbf{x}_t^{(j)} \mid \mathbf{x}_{t-1}^{(j)}, z_t^{(j)}, \theta)}_{\text{remaining emissions } (\in \mathbb{R}^{(\tilde{T}-1) \times K})} \right] \quad (\text{B.4})$$

where we have defined $\tilde{T} \triangleq T + 1$ to denote all timesteps after accounting for the zero-indexing. This variational factor can be considered as posterior of J conditionally independent Hidden Markov Models with autoregressive categorical emissions which recurrently feedback into the transitions. As per Sec. B.2, the transition function can be evaluated with $\mathcal{O}(TJL(K^2 + KDM_e))$ runtime complexity, where M_e is the dimension of the entity-level covariates, and where we have assumed that the evaluation of the entity-level recurrence function f takes DM_e operations, as it would if $f_\phi(\mathbf{x}_{t-1}^{(j)}, \mathbf{u}_{t-1}^{(j)}) = (\mathbf{x}_{t-1}^{(j)}, \mathbf{u}_{t-1}^{(j)})^T$. The evaluation of the emissions function is $\mathcal{O}(TJKD^2)$, assuming that the emissions distribution has a density that can be evaluated with $\mathcal{O}(D^2)$ operations at each timestep. Thus, by Props. A.2.1 and A.2.2, filtering and smoothing can be computed with $\mathcal{O}(TJ[K^2 + KD^2 + KDM_e])$ runtime complexity, under mild assumptions on the entity-level recurrence function and the emissions distribution. As a result, so can the computation of the unary and adjacent pairwise marginals necessary for the VEZ and M steps.

B.4 Updating the parameters

The M-step updates the transition parameters and emission parameters θ of our HSRDM given recent estimates of state-level posterior $q(s_{0:T})$ and entity-level posteriors $q(z_{0:T}^{(1:J)})$.

This update requires solving the following optimization problem

$$\theta = \underset{\theta}{\operatorname{argmax}} \mathcal{L}(\theta) \\ \text{where } \mathcal{L}(\theta) \triangleq \underbrace{\mathbb{E}_{q(s_{0:T}^{(1:J)})q(z_{0:T}^{(1:J)})} \left[\log p(\mathbf{x}_{0:T}^{(1:J)}, s_{0:T}^{(1:J)}, z_{0:T}^{(1:J)} \mid \theta) \right]}_{\text{expected log complete data likelihood}} + \underbrace{\log p(\theta)}_{\text{log prior}} \quad (\text{B.5})$$

Based on the structure of the model in Eq. (2.1), we can decompose this into separate optimization problems over the different model pieces $\theta = (\theta_{ss}, \theta_{es}, \theta_{ee}, \theta_{\text{init}})$ by assuming an appropriately factorized prior, as was done in Eq. (B.1).

To be concrete, for a HSRDM with transitions given by Eq. (2) and Gaussian vector autoregressive (Gaussian VAR) emissions

$$\mathbf{x}_t^{(j)} \mid \mathbf{x}_{t-1}^{(j)}, z_t^{(j)} \sim N \left(\mathbf{A}_j^{(z_t^{(j)})} \mathbf{x}_{t-1}^{(j)} + \mathbf{b}_j^{(z_t^{(j)})}, \mathbf{Q}_j^{(z_t^{(j)})} \right), \quad (\text{B.6})$$

as used in Secs. 5.1 and 5.2 we have

$$\theta_{ss} = (\mathbf{A}, \tilde{\mathbf{\Pi}}), \quad \theta_{es} = \{\Psi_j, \tilde{\mathbf{P}}_j\}_{j=1}^J, \quad \theta_{ee} = \{\{\mathbf{A}_{jk}, \mathbf{b}_{jk}, \mathbf{Q}_{jk}\}_{k=1}^K\}_{j=1}^J$$

Using this grouping of the parameters along with the complete data likelihood specification of Eq. (2.1) and the prior assumption in Eq. (B.1), we can decompose the objective as

$$\mathcal{L}(\theta) = \mathcal{L}_{\text{init}}(\theta_{\text{init}}) + \mathcal{L}_{ss}(\theta_{ss}) + \sum_{j=1}^J \mathcal{L}_{es}^{(j)}(\theta_{es}^{(j)}) + \mathcal{L}_{ee}^{(j)}(\theta_{ee}^{(j)})$$

We can then complete the optimization by separately performing M-steps for each of the subcomponents of θ . For example, to optimize the parameters governing the entity-level discrete state transitions $\theta_{es}^{(j)}$ for each entity $j = 1, \dots, J$, we only need to optimize

$$\begin{aligned} \mathcal{L}_{es}^{(j)}(\theta_{es}^{(j)}) &\triangleq \underbrace{\sum_{t=1}^T \mathbb{E}_{q(z_{0:T}^{(1:J)})q(s_{0:T})} \left[\log p(z_t^{(j)} | z_{t-1}^{(j)}, \mathbf{x}_{t-1}^{(j)}, s_t, \theta_{es}^{(j)}) \right]}_{\text{expected log entity discrete state transitions}} + \underbrace{\log p(\theta_{es}^{(j)})}_{\text{log prior}} \\ &= \sum_{t=1}^T \sum_{k, k'=1}^K \sum_{\ell=1}^L \log p(z_t^{(j)} = k' | z_{t-1}^{(j)} = k, \mathbf{x}_{t-1}^{(j)}, s_t = \ell, \theta_{es}^{(j)}) q(z_t^{(j)} = k', z_{t-1}^{(j)} = k) q(s_t = \ell) \\ &\quad + \log p(\theta_{es}^{(j)}) \end{aligned} \tag{B.7}$$

In particular, we do not require the variational posterior over the full entity-level discrete state sequence $q(z_{0:T}^{(1:J)})$, but merely the pairwise marginals $q(z_t^{(j)} = k', z_{t-1}^{(j)} = k)$, obtainable from the VEZ step in Eq. (3.2). Similarly, we do not require the variational posterior over the full system-level discrete state sequence $q(s_{0:T})$, but merely the unary marginals $q(s_t = \ell)$, obtainable from the VES step in Eq. (3.2).

The other components of θ are optimized similarly. In general, the optimization can be performed by gradient descent (e.g. using JAX for automatic differentiation [Bradbury et al., 2018]), although it can be useful to bring in closed-form solutions for the M substeps in certain special cases. For instance, when Gaussian VAR emissions are used as in Eq. (B.6), the entity emission parameters $\theta_{ee} = \{\{A_{jk}, b_{jk}, Q_{jk}\}_{k=1}^K\}_{j=1}^J$ can be estimated with closed-form updates using the sample weights $q(z_t^{(j)} = k)$ available from the VEZ-step.

B.5 Variational lower bound

A lower bound on the marginal log likelihood $\text{VLBO} \leq \log p(\mathbf{x}_{0:T}^{(1:J)})$, is given by

$$\text{VLBO}[\theta, q] = \underbrace{\mathbb{E}_q[\log p(\mathbf{x}_{0:T}^{(1:J)}, z_{0:T}^{(1:J)}, s_{0:T}, \theta)]}_{\text{energy}} + \underbrace{\mathbb{H}[q(z_{0:T}^{(1:J)}, s_{0:T})]}_{\text{entropy}} \tag{B.8}$$

The energy term $\mathbb{E}_q[\log p(\mathbf{x}_{0:T}^{(1:J)}, z_{0:T}^{(1:J)}, s_{0:T}, \theta)]$ is identical to the objective function for the M-step given in Eq. (B.5). Based on the structure of the model assumed in Eq. (2.1), the energy term decomposes into separate pieces for initialization, system transitions, entity transitions, and emissions. For example, see Eq. (B.7) for the piece relevant to entity transitions.

Now we consider computation of the entropy $\mathbb{H}[q(z_{0:T}^{(1:J)}, s_{0:T})]$ in Eq. (B.8). Since the variational factors $q(s_{0:T})$ and $\{q(z_{0:T}^{(j)})\}_{j=1}^J$ given respectively by the VES step in Sec. B.2 and the VEZ step in Sec. B.3 both have the form of rARHMMs , we can compute the entropy $\mathbb{H}[q(z_{0:T}^{(1:J)}, s_{0:T})] = \sum_{j=1}^J \mathbb{H}[q(z_{0:T}^{(j)})] + \mathbb{H}[q(s_{0:T})]$ via the entropy for rARHMMs that was provided in Sec. A.3.

B.6 Smart initialization

We can construct a “smart” (or data-informed) initialization of a HSRDM via the following two-stage procedure:

1. We fit J bottom-level rARHMMs , one for each of the J entities. In particular, the emissions for each bottom-level rARHMM are the emissions of the full HSRDM given in Eq. (2.4), and the transitions are the entity-level transitions given in Eq. (2.3).
2. We fit one top-level ARHMM . Here, the J emissions are the entity-level transitions given in Eq. (2.3). The transitions are the system-level transitions given in Eq. (2.2). The observations are taken to be the most-likely entity-level states as inferred by the bottom-level rARHMMs .

Below we give details on these initializations. In particular, both the bottom-level and top-level models *themselves* need initializations. We use the term *pre-initialization* to refer to the initializations of those models.

B.6.1 Initialization of bottom-level rARHMMs

Here we fit J bottom-level rARHMMs , one for each of the J entities, independently. In particular, the emissions for each bottom-level rARHMM are the emissions of the full HSRDM given in Eq. (2.4), and the transitions are the entity-level transitions given in Eq. (2.3).

Pre-initialization. The J bottom-level r ARHMMs *themselves* need good (data-informed) initializations. As an example, we describe the pre-initialization procedure in the particular case of Gaussian VAR emissions, as given in Eq. (B.6). In particular, we focus on a strategy for pre-initializing these emission parameters $\{\mathbf{A}_j^{(k)}, \mathbf{b}_j^{(k)}, \mathbf{Q}_j^{(k)}\}_{j,k}$, since the higher-level parameters in the model can be learned via the two-stage initialization procedure.

In particular, for each $j = 1, \dots, J$,

- a) We assign the observations $\mathbf{x}_{1:T}^{(j)}$ to one of K states by applying the K -means algorithm to either the observations themselves or to their velocities (discrete derivatives) $\mathbf{x}_{2:T}^{(j)} - \mathbf{x}_{1:T-1}^{(j)}$, depending upon user specification. We use the former choice in the FigureEight data, and the latter choice for basketball data.
- b) We then initialize the parameters by running separate vector autoregressions within each of the K clusters. In particular, for each state $k = 1, \dots, K$,
 - a) We find state-specific observation matrix $\mathbf{A}_j^{(k)}$ and biases $\mathbf{b}_j^{(k)}$ by applying a (multi-outcome) linear regression to predict $\mathbf{x}_t^{(j)}$ from the $\mathbf{x}_{t-1}^{(j)}$ whenever $\mathbf{x}_t^{(j)}$ belongs to the k -th cluster.
 - b) We estimate the regime-specific covariance matrices $\mathbf{Q}_j^{(k)}$ from the residuals of the above vector autoregression.

We initialize the entity-level transition parameters $\{\Psi_j, \tilde{\mathbf{P}}_j\}_{j=1}^J$ to represent a sticky transition probability matrix. This implies that we initialize $\Psi_j = \mathbf{0}$ for all j .

Expectation-Maximization. After pre-initialization, we estimate the J independent r ARHMMs by using the expectation maximization algorithm. Posterior state inference (i.e. the E-step) for this procedure is justified in Sec. A. Note that the posterior state inference for these bottom-level r ARHMMs can be obtained by reusing the VEZ step of Eq. (B.4) by setting the number of system states to $L = 1$.

B.6.2 Initialization of top-level ARHMM

Here we fit a *top-level* ARHMM. In particular, the emissions for the ARHMM are the entity-level transitions of the HSRDM given in Eq. (2.3), and the transitions of the ARHMM are the system-level transitions given in Eq. (2.2). We can perform posterior state inference for the top-level ARHMM by reusing the VES step of Eq. (B.3) with inputs being the posterior state beliefs on $z_{0:T}^{(1:J)}$ from the bottom-level r ARHMMs.

B.7 Multiple Examples

In some datasets, we may observe the same J entities over several distinct intervals of synchronous interaction. We call each separate interval of contiguous interaction an “example”. For example, the raw basketball dataset from Sec. 5.2 is organized as a collection of separate plays, where each play is one separate example. Between the end of one play and the beginning of the next, the players might have changed positions entirely, perhaps even having gone to the locker room and back for halftime.

Let E be the number of examples. Each example, indexed by $e \in \{1, 2, \dots, E\}$, starts at some reference time τ_e and has T_e total timesteps, covering the time sequence $t \in \{\tau_e, \tau_e + 1, \dots, \tau_e + T_e\}$. We’ll model each per-example observation sequence $\mathbf{x}_{\tau_e:\tau_e+T_e}^{(1:J)}$ as an iid observation from our HSRDM model.

To efficiently represent such data, we can stack the observed sequences for each example on top of one another. This yields a total observation sequence $\mathbf{x}_{0:T}^{(1:J)}$ that covers all timesteps across all examples, defining $T = T_1 + T_2 + \dots + T_E$. This representation doesn’t waste any storage on unobserved intervals between examples, easily accommodates examples of arbitrarily different lengths, and integrates well with modern vectorized array libraries in our Python implementation. As before in the single example case, our computational representation of $\mathbf{x}_{0:T}^{(1:J)}$ is as a 3-d array with dimensionality (T, J, D) .

For properly handling this compact representation, bookkeeping is needed to track where one example sequence ends and another begins. We thus track the ending indices of each example in this stacked representation: $\mathcal{E} = \{t_0, t_1, \dots, t_{E-1}, t_E\}$, where $-1 = t_0 < t_1 < t_2 < \dots < t_{E-1} < t_E = T$, and where $t_e = \tau_e + T_e$ is the last valid timestep observed in the e -th example for $e = 1, \dots, E$.

By inspecting the inference updates given above, including the filtering and smoothing updates for r ARHMM (see Props. A.2.1 and A.2.2), we find that we can handle this situation as follows:

- *E-steps (VEZ or VES)*: Whenever we get to a cross-example boundary, we replace the usual transition function with an initial state distribution. More concretely, the transition function for the VES step in Eq. (B.3) is modified so that any timestep t that represents the start of a new example sequence (that is, satisfies $t - 1 \in \mathcal{E}$) is replaced with π_s , and the transition function for the VEZ step in Eq. (B.4) at such timesteps is replaced with π_{z_j} . Similarly, the emissions functions at such timesteps are replaced with the initial emissions. This maneuver can be justified by noting that for any timestep t designating the onset of a new example, the initial state distributions play the role of \mathbf{A}_t and the initial emissions play the role of ϵ_t in Props. A.2.1 and A.2.2.
- *M-steps*: Due to the model structure, the objective function \mathcal{L} for the M-step can be expressed as a sum over timestep-specific quantities; for example, see Eq. (B.7). Thus, in the case of multiple examples, we simply adjust the set of timesteps over which we sum in the objective functions relative to each M substep. We update the entity emissions parameters θ_{ee} by altering the objective to sum over timesteps that *aren't* at the beginning of an example (so we sum over timesteps t where $t - 1 \notin \mathcal{E}$). We update the system state parameters θ_{ss} and entity state parameters θ_{es} by altering the objectives to sum only over timesteps that haven't straddled an example transition boundary. That is, we want to ignore any pair of timesteps $(t, t + 1)$ where $t \in \mathcal{E}$, so we again sum only over timesteps t where $t - 1 \notin \mathcal{E}$. Finally, we update the initialization parameters θ_{init} by altering the objective to sum over all timesteps that *are* at the beginning of an example.

C Methodology: Supplemental Information

Here we detail how we assess model fit (Sec. C.1) and compute forecasts (Sec. C.2). The primary difference between fitting and forecasting is that only the former has access to observations from evaluated entities over a time interval of interest. Hence, a good fit is more easily attained. A good forecast requires predictions of the discrete latent state dynamics without access to future observations, whereas fitting can use the future observations to infer the discrete latent state dynamics. However, model fit is still useful to investigate; for instance, it can be useful to determine if piecewise linear dynamics (including the choice of K , the number of per-entity states) provide a good model for a given dataset.

C.1 Model fit

To compute the fit of the model to $\{\mathbf{x}_t^{(j)}, \dots, \mathbf{x}_{t+u}^{(j)}\}$, the j -th entity's observed time series over some slice of integer-valued timepoints $[t, \dots, t + u]$, we initialize

$$\boldsymbol{\mu}_{t-1}^{(j)} = \mathbf{x}_{t-1}^{(j)}$$

And then forward simulate. In particular, for time τ in $[t, \dots, t + u]$, we do

$$\boldsymbol{\mu}_\tau^{(j)} \triangleq \sum_{k=1}^K q(z_\tau^{(j)} = k) \boldsymbol{\mu}_{\tau,k}^{(j)} \quad (\text{C.1})$$

where $\boldsymbol{\mu}_{\tau,k}^{(j)}$ is the conditional expectation of the emissions distribution from Eq. (2.4) with Radon-Nikodým density $p(\mathbf{x}_\tau^{(j)} | \mathbf{x}_{\tau-1}^{(j)} = \boldsymbol{\mu}_{\tau-1}^{(j)}, z_\tau^{(j)})$. For example, with Gaussian vector autoregressive (VAR) emissions, we have

$$\boldsymbol{\mu}_{\tau,k}^{(j)} \triangleq \mathbf{A}_{j,k} \boldsymbol{\mu}_{\tau-1,k}^{(j)} + \mathbf{b}_{j,k}$$

The resulting sequence $\{\boldsymbol{\mu}_t^{(j)}, \dots, \boldsymbol{\mu}_{t+u}^{(j)}\}$ gives the variational posterior mean for the j -th entity's observed time series over timepoints $[t, \dots, t + u]$.

C.2 Partial forecasting

By partial forecasting, we mean predicting $\{\mathbf{x}_t^{(j)}, \dots, \mathbf{x}_{t+u}^{(j)}\}_{j \in \mathcal{J}}$, the observed time series from some **to-be-forecasted entities** (with indices $\mathcal{J} \subset [1, \dots, J]$) over some forecasting horizon of integer-valued timepoints $[t, \dots, t + u]$, given observations $\{\mathbf{x}_t^{(j)}, \dots, \mathbf{x}_{t+u}^{(j)}\}_{j \in \mathcal{J}^c}$ from the **contextual entities** $\mathcal{J}^c \triangleq \{j \in [1, \dots, J] : j \notin \mathcal{J}\}$ over that same forecasting horizon, as well as observations from all entities over earlier time slices $\{\mathbf{x}_0^{(j)}, \dots, \mathbf{x}_{t-1}^{(j)}\}_{j \in [1, \dots, J]}$.

To instantiate partial forecasting, we must first adjust inference, and then perform a forward simulation.

1. *Inference adjustment.* The VEZ step (Sec. B.3) is adjusted so that the variational factors on the entity-level states over the forecasting horizon $\{q(z_t^{(j)}, \dots, z_{t+u}^{(j)})\}_j$ are computed only for the contextual entities $\{j \in \mathcal{J}^c\}$. Likewise, the VES step (Sec. B.2) is adjusted so that the variational factor on the system-level states over the forecasting horizon $q(s_t, \dots, s_{t+u})$ is computed from the observations $\{\mathbf{x}_t^{(j)}, \dots, \mathbf{x}_{t+u}^{(j)}\}_j$ and estimated entity-level states $\{q(z_t^{(j)}, \dots, z_{t+u}^{(j)})\}_j$ only from the contextual entities $\{j \in \mathcal{J}^c\}$. As a result, the M-step on the system-level parameters θ_{ss} automatically exclude information from the to-be-forecasted entities \mathcal{J} over the forecasting horizon $[t, \dots, t+u]$.
2. *Forward simulation.* Using the adjusted inference procedure from Step 1, we can use the Viterbi algorithm (or some other procedure) to obtain estimated system-states $\{\hat{s}_t, \dots, \hat{s}_{t+u}\}$ that do not depend on information from the to-be-forecasted entities \mathcal{J} over the forecasting horizon $[t, \dots, t+u]$. We then make forecasts by forward simulating. In particular, for time τ in $[t, \dots, t+u]$, we sample

$$z_t^{(j)} \sim p(z_t^{(j)} \mid z_{t-1}^{(j)}, \mathbf{x}_{t-1}^{(j)}, \hat{s}_t, \theta) \quad (\text{C.2})$$

$$\mathbf{x}_t^{(j)} \sim p(\mathbf{x}_t^{(j)} \mid \mathbf{x}_{t-1}^{(j)}, z_t^{(j)}, \theta) \quad (\text{C.3})$$

for all to-be-forecasted entities $j \in \mathcal{J}$.

Note in particular that the dependence of Eq. (C.2) upon \hat{s}_t allows our predictions about to-be-forecasted entities $\{j \in \mathcal{J}\}$ to depend upon observations from the contextual entities $\{j \in \mathcal{J}^c\}$ over the forecasting horizon.

D FigureEight Toy Data: Supplemental Information

D.1 Data generating process

Example D.1.1. (*FigureEight.*) Consider a model where we directly observe continuous observations $\mathbf{x}_{0:T}^{(1:J)}$, and where each $\mathbf{x}_t^{(j)} \in \mathbb{R}^2$ lives in the plane (i.e. $D = 2$). We form ‘‘Figure Eights’’ by having the observed dynamics rotate around an ‘‘upper circle’’ \mathcal{C}_1 with unit radius and center $\check{\mathbf{b}}^{(1)} \triangleq (0, 1)^T$ and a ‘‘lower circle’’ \mathcal{C}_2 with unit radius and center $\check{\mathbf{b}}^{(2)} \triangleq (0, -1)^T$. Entities tend to persistently rotate around one of these circles; however, when the observation approaches the intersection of the two circles $\mathcal{C}_1 \cap \mathcal{C}_2 = \{(0, 0)\}$, recurrent feedback can shift the entity’s dynamics into a new state (the other circle). These shifts occur only when the system-level state has changed; these shifts are not predictable from the entity-level time series alone. In particular, we have

$$\underbrace{s_t \mid s_{t-1}}_{\text{system transitions}} = h(s_t) \quad (\text{D.1a})$$

$$\underbrace{z_t^{(j)} \mid z_{t-1}^{(j)}, \mathbf{x}_{t-1}^{(j)}, s_t}_{\text{entity transitions}} \sim \text{Cat-GLM}_K \left(\underbrace{\boldsymbol{\eta}_t^{(j)}}_{\text{recurrence}} = \underbrace{\boldsymbol{\Psi}^{(s_t)}}_{\text{recurrence}} f(\mathbf{x}_{t-1}^{(j)}) + \underbrace{\tilde{\mathbf{P}}_j^T \mathbf{e}_{z_{t-1}^{(j)}}}_{\text{transitions}} \right) \quad (\text{D.1b})$$

$$\underbrace{\mathbf{x}_t^{(j)} \mid \mathbf{x}_{t-1}^{(j)}, z_t^{(j)}}_{\text{observation dynamics}} \sim N \left(\mathbf{A}_j^{(z_t^{(j)})} \mathbf{x}_{t-1}^{(j)} + \mathbf{b}_j^{(z_t^{(j)})}, \mathbf{Q}_j^{(z_t^{(j)})} \right) \quad (\text{D.1c})$$

Here, the notation used follows that of Eq. (2). Each line of this true data-generating process is explained in the corresponding paragraph below.

System-level state transitions. We take the number of system states to be $L = 2$. We set the system state chain $\{s_t\}_{t=1}^T$ through a deterministic process h which alternates states every 100 timesteps. We emphasize that in the *true* data-generating process, there is no recurrent feedback from observations x to system states s .

Entity-level state transitions. We set entity-specific baseline transition preferences to be highly sticky, $\mathbf{P}_j = \begin{bmatrix} p & (1-p) \\ (1-p) & p \end{bmatrix}$, where p is close to 1.0 (concretely, $p = .999$). By design, these preferences can be overridden when an entity travels near the origin. We choose the recurrence transformation $f : \mathbb{R}^D \rightarrow \mathbb{R}$ to be the radial basis function $f(\mathbf{x}) = \kappa \exp(-\frac{\|\mathbf{x}\|_2^2}{2\sigma^2})$, which returns a large value when the observation $\mathbf{x}_{t-1}^{(j)}$ is close to the origin. Similarly, we set the weight vector for these recurrent features to nudge observations near the origin to the system-preferred state. We set $\boldsymbol{\Psi}^{(\ell)} \in \mathbb{R}^K$ so entry $(\boldsymbol{\Psi}^{(\ell)})_k = a_{\text{high}}$ if the entity-level state k is preferred by the system-level state ℓ , and a_{low} otherwise, with $a_{\text{high}} \gg a_{\text{low}}$. Concretely, We set $a_{\text{high}} = 2$ and $a_{\text{low}} = -2$.

Emissions. To construct the entity-level emission distributions for each state (indexed by k), we choose $\mathbf{A}_j^{(k)} = \mathbf{A}_j$ to be a rotation matrix with angle $\theta = (-1)^r \frac{2\pi}{\tau_j}$ for all entity-level states k , where τ_j is the entity-specific periodicity and

$r \in \{0, 1\}$ determines the rotation direction. We may use a rotation matrix \mathbf{A} to rotate the observation around a center $\check{\mathbf{b}}$, by constructing dynamics of the form $\mathbf{A}(\mathbf{x} - \check{\mathbf{b}}) + \check{\mathbf{b}}$; therefore, to construct circle centers that are specific to entity-level states using Eq. (D.1c), we set $\mathbf{b}_j^{(k)} = (\mathbf{I} - \mathbf{A}_j)\check{\mathbf{b}}^{(k)}$ for all entities j and all entity-level states k . We set each of the observation noise covariance matrices $\mathbf{Q}_j^{(k)}$ to be diagonal, with diagonal entries equal to 0.0001.

△

D.2 Dataset

We simulate data from the *FigureEight* model (Example D.1.1), where there are $J = 3$ entities, each with $T = 400$ observations, where the periodicities for each entity are given by $(\tau_1, \tau_2, \tau_3) = (5, 20, 40)$. The generated sequences from one entity are shown in Fig. D.6.

D.3 Methods

HSRDM. We fit our HSRDM with transitions given in Eq. (2) and Gaussian vector autoregressive emissions as in Eq. (B.6). We set $L = K = 2$. We set the entity-level recurrence f to a Gaussian radial basis function and no system-level recurrence g . We perform inference as in Sec. B.

rAR-HMM. A collection of J rARHMM models can be fit as a special case of a HSRDM model where the number of system states is taken to be $L = 1$.

DSARF. We train the Deep Switching Autoregressive Factorization model [Farnoosh et al., 2021] with several different parameters. We train with several different choices of lags (l), spatial factors (S), discrete states (K), and learning rates, and find $l = [1, 2, 10, 11]$, $K = 5$, and $S = 5$ or $S = 10$ is preferred for capturing the dynamics across all channels. We set the same l , S and K for the complete independence, complete pooling and the multi-channel forecasting experiments.

Additionally, for the forecasting experiments, we fit this model 4 separate times, using distinct random seeds for each initialization, and choose the model with the largest ELBO after training for 500 epochs with learning rates of 0.01 and 0.05.

We perform long-term predictions, where we draw samples of the heldout observations from entity three from the generative model learned on the training set. To do this, we first fit the model to all 3 entities (all 400 time-points for entity 1 and entity 2 and upto time point 280 for entity 3). Time-points 280 to 400 in entity 3 are replaced with nan's during training, since our goal is to forecast at these time-points.

Once the model is trained, we use the learned parameters $\{\theta^s, \theta^w, \theta^F, \theta^z\}$ to draw forecasts via ancestral sampling from the DSARF generative model:

$$\begin{aligned} s_t &\sim p(s_t | s_{t-1}, \theta^s) \\ w_t &\sim p(w_t | w_{t-l}, s_t, \theta^w) \\ z &\sim p(z | \theta^z) \\ f_{1:K} &\sim p(F | z, \theta^F) \\ X_{280:400}^{forecast} &= [w_{280}, w_{281}, \dots, w_{400}]^T [f_1, f_2, \dots, f_K] \end{aligned}$$

D.4 Results

As mentioned in the main paper, here we show all 3 sample forecasts from various models. Figs. D.3, D.4, and D.5 show the sample forecasts from DSARF, rARHMM, and HSRDM, respectively. The sample forecasts are computed using partial forecasting (Sec. C.2).

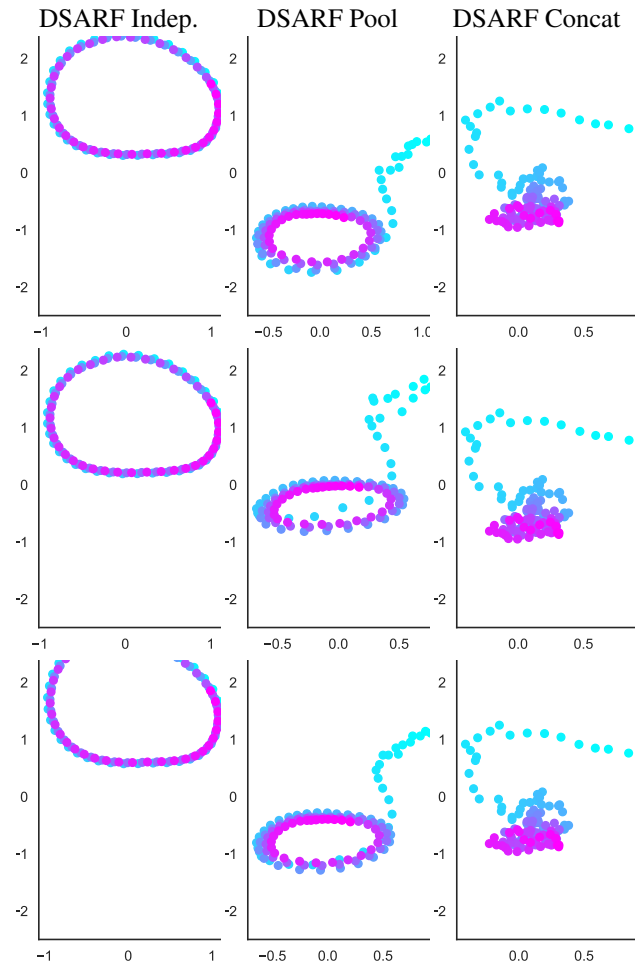


Figure D.3: Model predictions of heldout time segment of one entity in *Figure Eight* task. Shown are all 3 sampled partial forecasts from the DSARF baseline under each possible strategy (Indep., Pool, and Concat., defined in Sec. 5.1). Each column represents a different strategy. Each row represents a different model forecast.

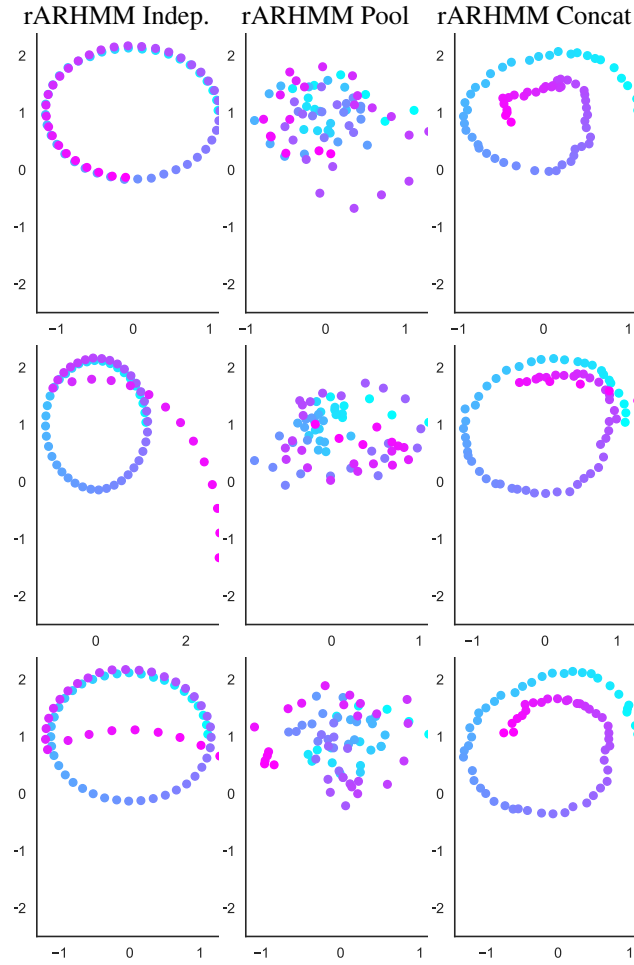


Figure D.4: Model predictions of heldout time segment of one entity in *Figure Eight* task. Shown are all 3 sampled partial forecasts from the rARHMM baseline under each possible strategy (Indep., Pool, and Concat., defined in Sec. 5.1). Each column represents a different strategy. Each row represents a different model forecast.

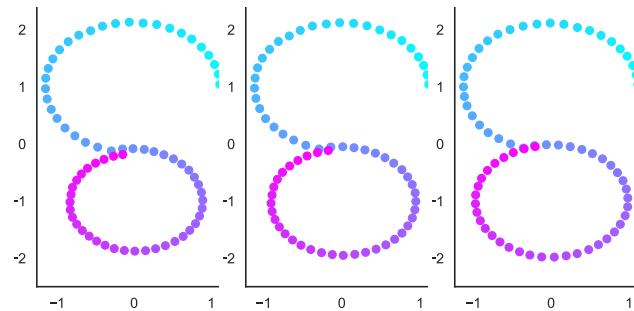


Figure D.5: Model predictions of heldout time segment of one entity in *Figure Eight* task. Shown are all 3 sampled partial forecasts from our HSRDM model. Each column represents a different model forecast.

Fig. D.6 shows the system- and entity-level state segmentations learned by the HSRDM model applied to the *FigureEight* dataset.

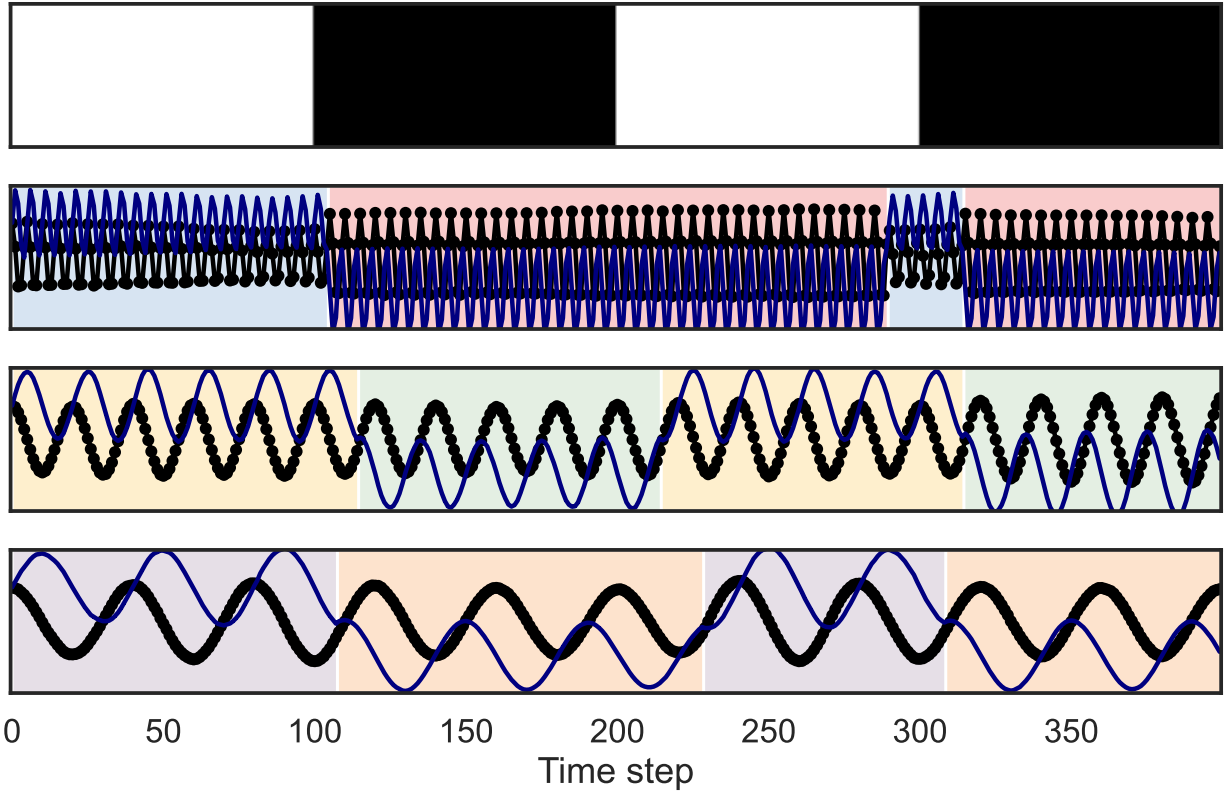


Figure D.6: *System- and entity-level state segmentations learned by the HSRDM model applied to the FigureEight dataset.* The top row gives the system-level segmentations. Each of the bottom three rows shows the time series from one of three entities, with superimposed entity-level state segmentations. The two dimensions of the time series are plotted with separate curves.

Although not shown here, we find that baseline models can fit the data well, despite having struggled to provide accurate forecasts. Here, the model fit is computed as the variational posterior mean trajectory, as given in Eq. (C.1). It is easier for models to fit the data than to forecast the future. A good fit can be attained so long as the model can learn how dramatic shifts in the observations suggest shifts in the underlying latent states. A good forecast requires predictions of the latent state dynamics without access to future observations.

Fig. D.8 shows the learned entity-level transition probability matrices (tpms) as function of the continuous observation $\mathbf{x}_t^{(3)}$ and the system-level state s_t . Here, we define an entity to be “far” from (or “close” to) the origin when $\mathbf{x}_t^{(j)}$ has a Euclidean distance to the origin that is in the 95th percentile (or 5th percentile, respectively), where the percentiles are taken w.r.t the sequence $\{\mathbf{x}_t^{(j)}\}_{t=1}^T$. We see that far from the origin, the HSRDM model assigns sticky tpms, but close to the origin, the entity is strongly pushed into either an UP observation or a DOWN observation, according to the system status s_t , which in this case is coordinating an (eventual) synchronization across entities. In contrast, a flat SRDM cannot coordinate the entities due to its lack of group-level switches. In this way, the HSRDM forecasts the future behavior of the entity $z_u^{(j)}$, $u > t$ by integrating three sources of information: (a) the entity’s (latent or physical) location $\mathbf{x}_{t-1}^{(j)}$, (b) the previous behavior of the entity $z_{t-1}^{(j)}$, and (c) the status of the full system s_t .

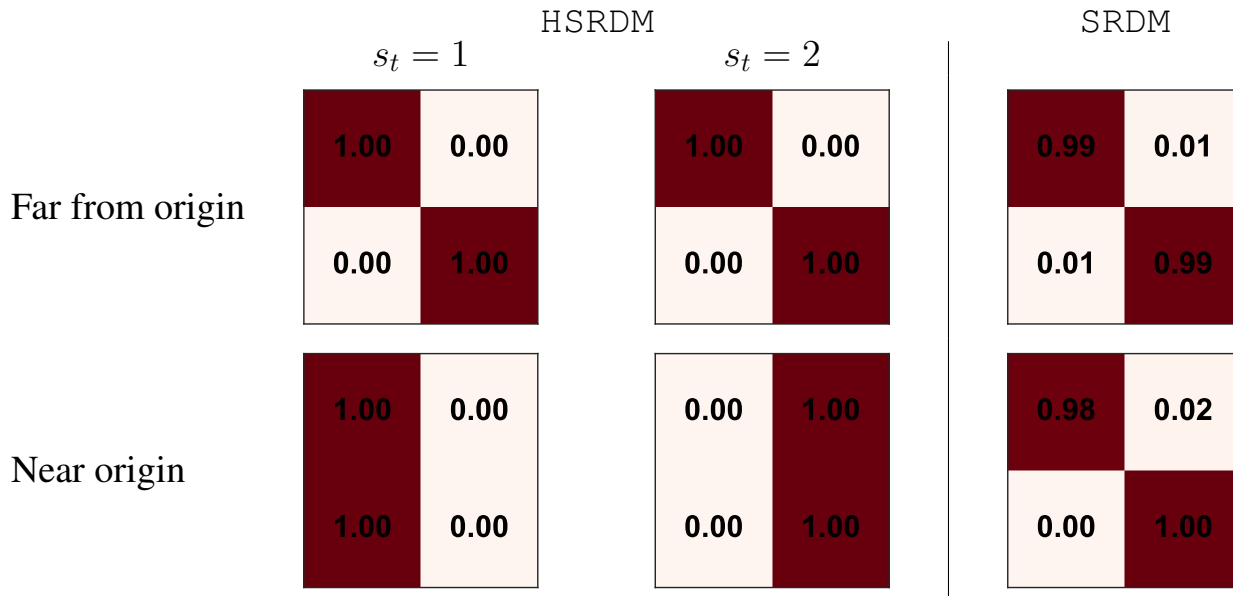


Figure D.8: Learned transition probability matrices for entity 3 as a function of distance to origin and system-level status s_t .

E Visual Security Experiment: Supplemental Information

For the visual security experiment, based on a quick exploratory analysis, we set $K = 4$ and $L = 3$. For the sticky Dirichlet prior on system-level transitions, as given in Eq. (B.2), we set $\alpha = 1.0$ and $\kappa = 50.0$, so that the prior would put most of its probability mass on self-transition probabilities between .90 and .99.

F Basketball Experiment: Supplemental Information

F.1 Dataset

Raw dataset. We obtain NBA basketball player location data for 636 games within the 2015-2016 NBA season from a publicly available repo [Linou, 2016]. Each sample provides the quarter of the game, number of seconds left in quarter, time on shot clock, (x,y,z) location of ball, and the (x,y) locations and IDs for the 10 players on the court. The court is represented as the rectangle $[0, 96] \times [0, 50]$ in the space of squared feet.

Selection of games. We focus on modeling the dynamics in games involving the Cleveland Cavaliers (CLE), the 2015-2016 NBA champions. In particular, out of 40 available games containing CLE, we investigate the 31 games containing one of the four most common starting lineups: 1. K. Irving - L. James - K. Love - J. Smith - T. Thompson; 2. K. Irving - L. James - K. Love - T. Mozgov - J. Smith; 3. L. James - K. Love - T. Mozgov - J. Smith - M. Williams; 4. M. Dellavedova - L. James - K. Love - T. Mozgov - J. Smith. Two games had data errors (lack of tracking or event data), which left a total of $G = 29$ games for analysis.

Downsampling. The raw data is sampled at 25 Hz. Following Alcorn and Nguyen [2021], we downsample to 5 Hz.

From plays to examples. The raw basketball dataset is represented in terms of separate *plays* (e.g. shot block, rebound offense, shot made). Following Alcorn and Nguyen [2021], we preprocess the dataset so that these plays are non-overlapping in duration. We also remove plays that do not contain one of CLE’s four most common starting lineups. For the purpose of unsupervised time series modeling, we then convert the plays into coarser-grained observational units. Although plays are useful for the classification task pursued by Alcorn and Nguyen [2021], play boundaries needn’t correspond to abrupt transitions in player locations. For example, the player coordinates are essentially continuous throughout shot block \rightarrow rebound offense \rightarrow shot made sequence mentioned above. Hence, we concatenate consecutive plays from the raw dataset until there is an abrupt break in player motion and/or a sampling interval longer than the nominal sampling rate. These observational units are called *events* in the main body of the paper (Sec. 5.2). Functionally, these observational units serve as *examples* (Sec. B.7). That is, when training models, each example is treated as an i.i.d. sample from the assumed model. For the remainder of the Appendix, we refer to these observational units as examples.

By construction, examples have a longer timescale than the plays in the original dataset. Examples typically last between 20 seconds and 3 minutes. For comparison, a `rebound offense` play takes a fraction of a second.

At the implementational level, we infer an example boundary whenever at least one condition below is met in a sequence of observations:

1. The wall clock difference between timesteps is larger than 1.2 times the nominal sampling rate.
2. The player’s step size on the court (given by the discrete derivative between two timesteps) is abnormally large with respect to either the court’s length or width, where abnormally large is defined as having an absolute z-score larger than 4.0.

Court rotation. The location of a team’s own basket changes at half time. This can switch can alter the dynamics on the court. We would like to control for the direction of movement towards the offensive and defensive baskets, as well as for player handedness. To control for this, we assume that the focal team (CLE)’s scoring basket is always on the left side of the court. When it is not, we rotate the court 180 degrees around the center of the basketball court. (Equivalently, we negate both the x and y coordinates with respect to the center of the court.) Since the basketball court has a width of 94 feet and a length of 50 feet, its center is located at (47, 25) when orienting the width horizontally. We prefer this normalization strategy to the random rotations strategy of [Alcorn and Nguyen \[2021\]](#), because the normalization strategy allows us to learn different dynamics for offense (movement to the left) and defense (movement to the right).

Index assignments. Each sample from our dataset gives the coordinates on the court of 10 players. Here we describe how we map the players to entity indices. Recall that we only model the plays that consist of starters from a focal team, CLE. We assign indices 0-4 to represent CLE starters, and indices 5-9 to represent opponents.

Index assignment for CLE is relatively straightforward. Although we model plays from the G games involving four different starting lineups, we can consistently interpret the indices as 0: `Lebron James`, 1: `Kevin Love`, 2: `J.R. Smith`, 3: `Starting Center`, 4: `Starting Guard`. Depending on the game, the starting center was either T. Mazgov or T. Thompson. Similarly, the starting guard was either K. Irving, M. Williams, or M. Dellavedova.

Index assignment for the opponents is more involved. The opponent teams can vary from game to game, and even a fixed team substitutes players throughout a game. There are numerous mechanisms for assigning indices in the face of such *player substitutions* [[Raabe et al., 2023](#)]. Although role-based representations are popular (e.g. see [[Felsen et al., 2018](#)] or [[Zhan et al., 2019](#)]) because they capture invariants lost within identity-based representations [[Lucey et al., 2013](#)], we used a simple heuristic whereby we assign indices 5-9 based on the the player’s typical positions. The typical positions can be scraped from Wikipedia. We let the model discover dynamically shifting roles for the players via its hierarchical discrete state representation.

One complication in assigning indices from these position labels is that the provided labels commonly blend together multiple positions (e.g. ‘Shooting guard / small forward’ or ‘Center / power forward’). Should the second player be labeled as a center or a forward? What if there are multiple centers? How do we discriminate between two forwards? To solve such problems, we proceed as follows, operating on a play-by-play basis

1. *Assign players to coarse position groups.* We first assign players to coarse position groups (forward, guard, center). We assume that each play has 2 forwards, 1 center, and 2 guards. We use indices 5-6 to represent the forwards, index 7 to represent the center, and indices 8-9 to represent the guards. As noted above, a given player can be multiply classified into a coarse position group; however, a reasonable assignment for a player can be made by considering the position labels for the other players who are on the court at the same time. To do this, we form B , a 5×3 binary matrix whose rows are players on the team and whose columns represent the coarse position groups. An entry in the matrix is set to True if the player is classified into that position group. We start with the rarest position group (i.e. the column in B with the smallest column sum) and assign players to that position group, starting with players who have the least classifications (i.e. the players whose rows in B have the smallest row sum). Ties are broken randomly. We continue until we have satisfied the specified assignments (2 forwards, 1 center, and 2 guards). If it is not possible to make such coarse assignments, we discard the play from the dataset.
2. *Order players within the coarse position groups.* This step only needs to be performed for forwards and guards, since there is only 1 ordering of the single center. We define an arbitrary ordering of forward positions by

```
FORWARD_POSITIONS_ORDERED = [
```

```

    "Small forward / shooting guard",
    "Small forward / point guard",
    "Small forward",
    "Small forward / power forward",
    "Power forward / small forward",
    "Power forward",
    "Power forward / center",
    "Center / power forward",
    "Shooting guard / small forward",
]

```

and guard positions by

```

GUARD_POSITIONS_ORDERED = [
    "Small forward / shooting guard",
    "Shooting guard / small forward",
    "Shooting guard",
    "Shooting guard / point guard",
    "Point guard / shooting guard",
    "Point guard",
    "Combo guard",
]

```

For each players assigned to a position group in $\{forward, guard\}$, we order the players in terms of their location of their position on the above lists. Ties are broken randomly.

Normalization To assist with initialization and learning of parameters, we normalize the player locations on the court from the rectangle $[0, 96] \times [0, 50]$ in units of feet to the unit square $[0, 1] \times [0, 1]$.

F.2 Evaluation strategy

We divide the $G = 29$ total games into 20 games to form a candidate training set, 4 games to form a validation set (for setting hyperparameters), and 5 games to form a test set. Of the first 20 games within our candidate training set, we construct small (1 game), medium (5 games), and large (20 games) training sets. The small, medium, and large training sets contained 20, 215, and 676 examples, respectively.

The test set contained 158 examples overall. However, we required that each example be at least 10 seconds long (i.e. 50 timesteps) to be included in the evaluation run. This exclusion criterion left $E = 75$ examples. For each such example, we uniformly select a timepoint $T^* \in [T_{\min\text{-context-length}}, T - T_{\text{forecast-length}}]$ to demarcate where the context window ends. We set $T_{\min\text{-context-length}} = 4$ seconds (i.e. 20 timesteps) and $T_{\text{forecast-length}} = 6$ seconds (i.e. 30 timesteps). The first $[0, T^*]$ seconds are shown to the trained model as context, and forecasts are made within the forecasting window of $\mathcal{F} := [T^* + 1, T^* + T_{\text{forecast-length}}]$ seconds.

For a fixed example e , forecasting sample s , player j , and forecasting method m , we summarize the error in a forecasted trajectory by **mean forecasting error** (MFE)

$$\text{MFE}_{m;e,s,j} \triangleq \frac{1}{|\mathcal{F}|} \sum_{t \in \mathcal{F}} \sqrt{\sum_{d=0}^1 (\hat{x}_{e,t,j,d,m,s} - x_{e,t,j,d})^2} \quad (\text{F.1})$$

where $x_{e,t,j,d}$ is the true observation on example e at time t for player j on court dimension d , and $\hat{x}_{e,t,j,d,m,s}$ is the forecasted observation by forecasting sample s using forecasting method m . So $\text{MFE}_{m;e,s,j}$ gives the average distance over the forecasting window between the forecasted trajectory and the true trajectory.

To quantify the performance of a forecasting methods, we can define a model's *example-wise* mean forecasting error as

$$\text{MFE}_{m;e} \triangleq \frac{1}{SJ} \sum_{s=1}^S \sum_{j=1}^J \text{MFE}_{m;e,s,j} \quad (\text{F.2})$$

Taking the mean of $\text{MFE}_{m;e}$ and its standard error lets us quantify a model's typical squared forecasting error on an example,

as well as our uncertainty, with

$$\text{MFE}_m \triangleq \frac{1}{E} \sum_{e=1}^E \text{MFE}_{m;e} \quad (\text{F.3})$$

$$\sigma(\text{MFE}_m) \triangleq \frac{\sqrt{\sum_{e=1}^E (\text{MFE}_{m;e} - \text{MFE}_m)^2}}{E} \quad (\text{F.4})$$

Although in Sec. F.1, we described normalization of basketball coordinates to the unit square for the purpose of model initialization and training, when evaluating models, we convert the forecasts and ground truth back to unnormalized coordinates, so that MFE has units of feet. That is, we represent observations $x_{e,t,j,d}$ and forecasts $\hat{x}_{e,t,j,d,m,s}$ on the basketball court (of size $[0, 94] \times [0, 50]$ feet). Thus $\sqrt{\text{MSE}_m}$ can be interpreted as a model’s typical amount of error in feet on the court at a typical timepoint in the forecasting window (but of course forecasting error tends to be lower at timepoints closer to T^* than farther from T^*).

F.3 Models

F.3.1 Overview of Models

We compare the performance of our HSRDM against a number of baselines, giving the modeling strategies below. For details on each strategy, see Sec. F.3.2.

1. **HSRDM**. This is our *hierarchical switching recurrent dynamical model*, as presented in Sec. 2.
2. **rARHMMs**. By ablating the top-level discrete "game" states (i.e., the system-level switches) in the HSRDM, we obtain 10 independent rARHMMs [Linderman et al., 2017], one for each player.
3. **HSDM**. By ablating the multi-level recurrence from the HSRDM, we obtain a *hierarchical switching dynamical model*.
4. **AgentFormer** is a transformer-inspired stochastic multi-agent (i.e. multi-entity) trajectory prediction model.
5. **Fixed velocity**. Here we compute each player’s velocity from the two timesteps immediately prior to the forecasting window \mathcal{F} , and take this velocity to be constant throughout \mathcal{F} . This is a common, and often surprisingly competitive, naive baseline for multi-agent models; e.g. see [Yeh et al., 2019].

F.3.2 Modeling Details

HSRDM. Here we model $J = 10$ basketball player trajectories on the court with an HSRDM with Gaussian vector autoregressive emissions; that is, we use

$$\underbrace{s_t \mid s_{t-1}, \mathbf{x}_{t-1}^{(1:J)}}_{\text{system transitions}} \sim \text{Cat-GLM}_L \left(\underbrace{\tilde{\Pi}^T e_{s_{t-1}}}_{\text{endogenous transition preferences}} + \underbrace{\Lambda g_\psi(\mathbf{x}_{t-1}^{(1:J)}, \mathbf{v}_{t-1})}_{\text{bias from recurrence and covariates}} \right) \quad (\text{F.5})$$

$$\underbrace{z_t^{(j)} \mid z_{t-1}^{(j)}, \mathbf{x}_{t-1}^{(j)}, s_t}_{\text{entity transitions}} \sim \text{Cat-GLM}_K \left(\underbrace{(\tilde{P}_j^{(s_t)})^T e_{z_{t-1}^{(j)}}}_{\text{endogenous transition preferences}} + \underbrace{\Psi_j^{(s_t)} f_\phi(\mathbf{x}_{t-1}^{(j)}, \mathbf{u}_{t-1}^{(j)})}_{\text{bias from recurrence and covariates}} \right) \quad (\text{F.6})$$

$$\underbrace{\mathbf{x}_t^{(j)} \mid \mathbf{x}_{t-1}^{(j)}, z_t^{(j)}}_{\text{observation dynamics}} \sim N \left(\mathbf{A}_j^{(z_t^{(j)})} \mathbf{x}_{t-1}^{(j)} + \mathbf{b}_j^{(z_t^{(j)})}, \mathbf{Q}_j^{(z_t^{(j)})} \right) \quad (\text{F.7})$$

where $\mathbf{x}_t^{(j)} \in ([0, 1] \times [0, 1])$ gives player j ’s location on the normalized basketball court at timestep t .

Our system-level recurrence $g_\psi(\mathbf{x}_{t-1}^{(1:J)}, \mathbf{v}_{t-1}) = \mathbf{x}_{t-1}^{(1:J)}$ reports *all* player locations $\mathbf{x}_i^{(1:J)}$ to the system-level transition function, allowing the probability of latent game states to depend on player locations. Inspired by Linderman et al. [2017], our entity-level recurrence function $f_\phi(\mathbf{x}_{t-1}^{(j)}, \mathbf{u}_{t-1}^{(j)}) = (\mathbf{x}_{t-1}^{(j)}, \mathbb{I}[\mathbf{x}_{t-1,0}^{(j)} < 0.0], \mathbb{I}[\mathbf{x}_{t-1,0}^{(j)} > 1.0], \mathbb{I}[\mathbf{x}_{t-1,1}^{(j)} < 0.0], \mathbb{I}[\mathbf{x}_{t-1,1}^{(j)} > 1.0])^T$, where $\mathbf{x}_{i,d}^{(j)}$ is the d -th coordinate of $\mathbf{x}_i^{(j)}$ and $\mathbb{I}[\cdot]$ is the indicator function, reports an individual player’s location $\mathbf{x}_{t-1}^{(j)}$ (and out-of-bounds indicators) to that player’s entity-level transition function, allowing each player’s probability of remaining in autoregressive regimes to vary in likelihood over the court.

We set the number of system and entity states to be $L = 5$ and $K = 10$ based on informal experimentation with the training set; we leave formal setting of these values based on the validation set to future work. For the sticky Dirichlet prior on system-level transitions, as given in Eq. (B.2), we set $\alpha = 1.0$ and $\kappa = 50.0$ so that the prior would put most of its probability mass on self-transition probabilities between .90 and .99.

We initialize the model using the smart initialization strategy of Sec. B.6. We pre-initialize the entity emissions parameters θ_{ee} by applying the k -means algorithm to each player’s discrete derivatives (so long as consecutive timesteps do not span an example boundary). We pre-initialize the entity state parameters θ_{es} by setting \tilde{P} to be the log of a sticky symmetric transition probability matrix with a self-transition probability of 0.90, and by drawing the entries of $\tilde{\Psi}$ i.i.d from a standard normal. We pre-initialize the system state parameters θ_{ss} by setting $\tilde{\Pi}$ to be the log of a sticky symmetric transition probability matrix with a self-transition probability of 0.95, and by drawing the entries of $\tilde{\Lambda}$ i.i.d from a standard normal. We pre-initialize the initialization parameters θ_{init} by taking the initial distribution to be uniform over system states, uniform over entity states for each entity, and standard normal over initial observations for each entity and each entity state. We execute the two-stage initialization process via 5 iterations of expectation-maximization for the J bottom-half $rARHMMs$, followed by 20 iterations for the top-half $ARHMM$.

We run our CAVI algorithm for 2 iterations, as informal experimentation with the training set suggested this was sufficient for approximate ELBO stabilization.

$rARHMMs$. By ablating the top-level discrete "game" states (i.e., the system-level switches) in the HSRDM, we obtain independent $rARHMMs$ [Linderman et al., 2017], one for each of the $J = 10$ players. More specifically, by removing the system transitions in Eq. (F.5) from the model, the entity transitions simplify as $p(z_t^{(j)} | z_{t-1}^{(j)}, \mathbf{x}_{t-1}^{(j)}, s_t) = p(z_t^{(j)} | z_{t-1}^{(j)}, \mathbf{x}_{t-1}^{(j)})$, because the entity transition parameters simplify as $\tilde{P}_j^{(st)} = \tilde{P}_j$ and $\tilde{\Psi}_j^{(st)} = \tilde{\Psi}_j$. As a result, the J bottom-level $rARHMMs$ are decoupled. Implementationally, this procedure is equivalent to an HSRDM with $L = 1$ system states. Initialization and training is otherwise performed identically as with HSRDM.

HSDM By ablating the multi-level recurrence from the HSRDM, we obtain a *hierarchical switching dynamical model* (HSDM). This can be accomplished by setting $g_\psi \equiv 0$ in Eq. (F.5) and $f_\phi \equiv 0$ in Eq. (F.6). Initialization and training is otherwise performed identically as with HSRDM.

Agentformer. AgentFormer [Yuan et al., 2021] is a multi-agent (i.e. multi-entity) variant of a transformer model whose forecasts depend upon both temporal and social (i.e. across-entity) relationships. Unless otherwise noted, we follow Yuan et al. [2021] in determining the training hyperparameters. In particular, our prediction model consists of 2 stacks of identical layers for the encoder and decoder with a dropout rate of 0.1. The dimensions of keys, queries and timestamps for the agentformer are set to 16, while the hidden dimension of the feedforward layer is set to 32. The number of heads for the multi-head agent aware attention is 8 and all MLPs in the model have a hidden dimension of (512, 256). The latent code dimension of the CVAE is set to 32, and the agent connectivity threshold is set to 100. Because the basketball training datasets have many more examples than the pedestrian trajectory prediction experiments in Yuan et al. [2021] (which only have 8 examples), we train the agentformer model and the DLow trajectory sampler for 20 epochs each (rather than 100) to keep the computational load manageable. We therefore apply the Adam optimizer with learning rate of 10^{-3} rather than 10^{-4} to accommodate the reduced number of epochs. Also, to match the specifications of the evaluation strategy from Sec. F.2, we set the number of future prediction frames during training to 30, and the number of diverse trajectories sampled by the trajectory sampler to 20. We ensure convergence by tracking the mean-squared error.

F.4 Future directions

Opportunities abound for improving the ability of HSRDM to model basketball trajectories. Here we provide some examples:

1. *Utilize covariates within transition functions.* Note from Sec. F.3.2 that covariates were not used in the recurrence functions. Other instantiations of Eq. (2) might consider using useful covariates, such as the coordinates of the ball.
2. *Make recurrence functions more informative.* Raabe et al. [2023] describe expert features determined by the sports analytics community to be useful for forecasting basketball trajectories. These features could be useful to incorporate within the system-level and entity-level transition functions. For instance, Raabe et al. [2023, Table 2, pp.3795] present two game-level features, *team ball distance* and *inter team distance*, which could provide useful information to the $\mathbf{x}^{(1:J)}$ -to- s system-level recurrence function. Similar remarks could be made about utilizing player-level features from Raabe et al. [2023] to inform the $\mathbf{x}^{(j)}$ -to- $z^{(j)}$ entity-level recurrence functions.

3. *Use higher-order recurrence functions.* Our current instantiations of HSRDM uses first-order recurrence by feeding back player *locations* into state transition functions. By extending to second-order recurrence, we could feed back player *derivatives* to state transition functions, which might provide valuable additional information about where the players will go next.
4. *Recognize court boundaries more directly.* The current instantiation of HSRDM respects enforces court boundaries indirectly, via the linear entity-level recurrence function of [Linderman et al., 2017] and via biasing entity-level transitions with weighted out-of-bounds indicators. As seen in Sec. 5.2, this strategy does reduce the probability of wildly out-of-bounds forecasts. However, the court boundaries could perhaps be enforced more directly by forecasting with Gaussian vector autoregressions that are truncated, either post-hoc after training [Wojnowicz et al. 2023] or during training itself. Note the complication that players do sometimes run out of bounds, although not as often or as much as happens during some of the forecasts made by any of the modeling strategies we studied.

Further improvements to modeling basketball could perhaps be obtained by expanding the HSRDM to include an additional $z^{(1:J)}$ -to- s recurrence, which might be called a *top-level recurrence*. Such recurrence might naturally accommodate certain features from [Raabe et al. 2023] such as *team stretch index* and *team separateness*.

G Code

Source code for running HSRDM and partially reproducing the experiments in this paper can be found at <https://github.com/mikewojnowicz/dynagroup>.